



Available online at [www.sciencedirect.com](http://www.sciencedirect.com)

**ScienceDirect**

Geochimica et Cosmochimica Acta 319 (2022) 318–336

**Geochimica et  
Cosmochimica  
Acta**

[www.elsevier.com/locate/gca](http://www.elsevier.com/locate/gca)

# Widespread lithogenic control of marine authigenic neodymium isotope records? Implications for paleoceanographic reconstructions

A.N. Abbott <sup>a,b,\*</sup>, S.C. Löhr <sup>a,c</sup>, A. Payne <sup>a,d</sup>, H. Kumar <sup>a</sup>, J. Du <sup>e</sup>

<sup>a</sup> Macquarie University, Department of Earth and Environmental Sciences, North Ryde, New South Wales 2109, Australia

<sup>b</sup> Now at Department of Marine Science, Coastal Carolina University, USA

<sup>c</sup> Department of Earth Sciences, University of Adelaide, Australia

<sup>d</sup> Now at the Department of Environmental Systems Sciences, ETH Zürich, Switzerland

<sup>e</sup> Institute of Geochemistry and Petrology, Department of Earth Sciences, ETH Zürich, Switzerland

Received 19 April 2021; accepted in revised form 19 November 2021; Available online 27 November 2021

---

## Abstract

Our understanding of past ocean-climate dynamics is informed by multiple paleocirculation proxies including  $\delta^{13}\text{C}$ ,  $^{231}\text{Pa}/^{230}\text{Th}$ , and radiogenic neodymium isotopes ( $\varepsilon_{\text{Nd}}$ ). Of these, the  $\varepsilon_{\text{Nd}}$  signature of marine authigenic phases is of particular importance as it is considered a robust circulation proxy applicable across timescales, permitting circulation reconstructions during periods of rapid, climatically-induced biological or chemical change (e.g. productivity, pH). However, growing evidence of non-conservative behavior and a widespread sedimentary source (benthic flux via pore water) of Nd to the global ocean suggests that authigenic  $\varepsilon_{\text{Nd}}$  records do not strictly record a water mass signature, highlighting the need to reconsider interpretations of the authigenic record. To examine the impact of a sedimentary influence on the authigenic record, here we compile paired authigenic and detrital neodymium records from every major ocean basin and from 80 Ma to present. We then focus on just the North Atlantic Ocean basin to examine if this relationship holds up regionally and how authigenic  $\varepsilon_{\text{Nd}}$  changes relate to sediment composition changes from two scientific ocean drill cores spanning the past 25 ka. We present a new conceptual framework to guide our discussion that examines the coupling or decoupling of authigenic and detrital  $\varepsilon_{\text{Nd}}$  in terms of the relative importance of each of the three major potential controls as defined in the existing literature (bottom water, pore water, sediments) on the authigenic record. Our compilation reveals a strong linear relationship between detrital  $\varepsilon_{\text{Nd}}$  and authigenic  $\varepsilon_{\text{Nd}}$  (correlation coefficient = 0.86,  $n = 871$ ), demonstrating a widespread influence of lithogenically sourced neodymium on authigenic  $\varepsilon_{\text{Nd}}$ . We find the same is true within the North Atlantic, with the authigenic records at both locations strongly influenced by the sediments and likely not recording bottom water neodymium values. Emerging evidence for a lithogenic or benthic flux influence on the budgets of a wide range of trace elements suggests that our interpretative framework will be broadly useful for understanding the behavior of trace elements and their isotopes at the sediment-water interface.

© 2021 Elsevier Ltd. All rights reserved.

**Keywords:** Neodymium isotopes; Rare earth elements; Benthic flux; Paleoceanography; Pore water

---

**Abbreviations:** SEM, Scanning Electron Microscope; ODP, Ocean Drilling Program; IODP, International Ocean Discovery Program; IRD, Ice Rafted Debris; LGM, Last Glacial Maximum; XRD, X-Ray Diffractometer; EDS, Energy Dispersive Spectroscopy

\* Corresponding author at: Coastal Carolina University, Department of Marine Sciences, Conway, SC 29526 USA.

E-mail address: [abbot152@d.umn.edu](mailto:abbot152@d.umn.edu) (A.N. Abbott).

## 1. INTRODUCTION

The  $\varepsilon_{\text{Nd}}$  signature of authigenic sedimentary phases is widely used for reconstructions of ocean circulation. These authigenic records come from various archives, with sediment leaches, fish teeth/debris, and foraminifera being the most commonly used in paleoceanography. The radiogenic neodymium isotopic signature, expressed as  $\varepsilon_{\text{Nd}} [{}^{143}\text{Nd}/{}^{144}\text{Nd}]$  normalized to the Chondritic Uniform Reservoir] (Jacobsen and Wasserburg, 1980), is recovered from authigenic archives using targeted chemical extraction procedures. The central assumptions underpinning the use of  $\varepsilon_{\text{Nd}}$  as a circulation proxy are that water mass  $\varepsilon_{\text{Nd}}$  is 1) geographically distinct based on water mass origin, 2) quasi-conservative, and 3) imprinted on, and can be recovered reliably from, authigenic archives (Frank, 2002). Where these assumptions are met, the  $\varepsilon_{\text{Nd}}$  proxy provides unique constraints on the movement and origin of water masses during critical periods of earth history (e.g. Rutberg et al., 2000; Scher and Martin, 2004; Roberts et al., 2010; van de Flierdt et al. 2016; Basak et al., 2018; McKinley et al., 2019).

The close correspondence between bottom water  $\varepsilon_{\text{Nd}}$  and the ‘authigenic’  $\varepsilon_{\text{Nd}}$  signature (see recent compilation in Tachikawa et al. 2017) recovered from fish debris, foraminifera (Elmore et al., 2011), or Fe-Mn oxyhydroxide phases (operationally defined through sediment leaching; Blaser et al., 2016) in core top samples is widely considered to support the view that the authigenic signature is a robust proxy with which to reconstruct paleo-bottom water  $\varepsilon_{\text{Nd}}$  and hence infer ocean circulation (e.g. Frank, 2002; Gutjahr et al., 2008; Roberts et al., 2010), with changes in authigenic  $\varepsilon_{\text{Nd}}$  over time interpreted to record changes to water mass origin. However, discrepancies around both the assumption of isotopic conservation in seawater and around whether the authigenic phases are recording bottom water or something else are problematic to the utility of  $\varepsilon_{\text{Nd}}$  as a water mass tracer. Challenging the assumption that neodymium isotopes behave quasi-conservatively in seawater are observations of non-conservative behavior of Nd including a growing body of evidence for the mobilization of neodymium during early sediment diagenesis, both in shallow- and deep-water settings (Jeandel et al., 2007; Wilson et al., 2012; Pearce et al., 2013; Abbott et al., 2015a; Roberts and Piotrowski, 2015; Abbott et al., 2016; Du et al., 2016; Howe et al., 2016; Jeandel, 2016; Haley et al., 2017; Abbott, 2019). Furthermore, global ocean circulation models that consider seawater  $\varepsilon_{\text{Nd}}$  distributions require an additional neodymium source in the deep ocean to reconcile the models’ seawater  $\varepsilon_{\text{Nd}}$  predictions with modern observations, identifying up to 95% of the source of neodymium to the ocean as missing (Tachikawa et al., 2003; Arsouze et al., 2009; Jones et al., 2008; Rempfer et al., 2011; Gu et al. 2019). Importantly, initial pore water measurements have shown that a benthic Nd source can account for an amount consistent with the ‘missing’ neodymium in the global budgets (Arsouze et al., 2009; Abbott et al., 2015a; Abbott, 2019). All of the above observations, including the core top authigenic correspondence to bottom water  $\varepsilon_{\text{Nd}}$ , can be reconciled with a shift to a ‘bottom-up’

benthic source model to describe neodymium in the ocean (Haley et al., 2017), where the agreement between bottom water  $\varepsilon_{\text{Nd}}$  and the ‘authigenic’  $\varepsilon_{\text{Nd}}$  signatures is a predictable consequence of a spatially widespread, large benthic flux (Du et al., 2016; Abbott et al., 2019; Du et al., 2020).

These observations do not just bring into question the quasi-conservative behavior of Nd in seawater, but also have implications for what is ultimately recorded in the sedimentary archives. The high Nd concentrations of the pore water driving a benthic flux are in contact with the authigenic phases throughout early diagenesis, suggesting these archives may record reactive sediment phases via the pore water instead of a seawater signature (Abbott et al., 2016). For instance, even tiny amounts ( $\sim 0.0000001\%$ ) of sediment dissolution have been demonstrated to be able to shift the  $\varepsilon_{\text{Nd}}$  of the pore water from ambient seawater to that recorded in fish teeth on the Adélie shelf near site U1356 (Huck et al., 2016) and similar pore water influences are expected for foraminifera during early diagenesis (Palmer and Elderfield, 1985, 1986; Skinner et al., 2019). Even if the overlying water column sets the signature, any non-conservative change to bottom water would have similar implications for the deposited authigenic record (e.g. Roberts and Piotrowski, 2015; Howe et al., 2016; Jaume-Sequí et al., 2021). Additional complications arise with the sediment leach archive as the phase associated with the recovered neodymium is often only able to be operationally defined, meaning in some cases the phase reacting with leach solutions is not the intended phase of interest. For example, recent high-resolution SEM analyses have demonstrated that the Fe-Mn oxyhydroxide phases meant to be targeted by reductive leaching are not ubiquitous in marine sediments, and instead the leached signature associated with iron may be controlled by clay mineral dissolution (Abbott et al., 2019). Even when the phase of interest is present, leaching techniques are highly variable and prone to releasing unintentional sediment phases (e.g. clays, volcanic debris; Roberts et al., 2010; Wilson et al., 2012; Wilson et al. 2013; Du et al. 2016; Abbott et al., 2019; McKinley et al., 2019; supplemental table 1).

Despite these uncertainties with respect to the controls of the authigenic  $\varepsilon_{\text{Nd}}$  record and increasing evidence for a sedimentary influence, authigenic  $\varepsilon_{\text{Nd}}$  shifts continue to often be interpreted as strictly a tracer of ocean circulation. Authigenic  $\varepsilon_{\text{Nd}}$  shifts often align with independently documented climatic and ocean reorganizations, and this has encouraged the idea that the compromising influence of non-conservative processes (such as boundary exchange or reactive detritus) is spatially or temporary limited (e.g. Jeandel et al., 2007; Gutjahr et al., 2008; Wilson et al., 2012; Pearce et al., 2013; Osborne et al., 2014; Böhm et al., 2015; Rousseau et al., 2015; Howe et al., 2016; Blaser et al., 2019; Vogt-Vincent et al., 2020). The fundamentally different relationships expected between the bottom water, the authigenic  $\varepsilon_{\text{Nd}}$  records, and the sediment composition (detrital or bulk sediment  $\varepsilon_{\text{Nd}}$ ) in the two competing ‘top-down’ and ‘bottom up’ models provide a way to evaluate the importance of each via comparison of paired authigenic and detrital  $\varepsilon_{\text{Nd}}$  records. Here, we present a

new global compilation of published authigenic and detrital  $\varepsilon_{\text{Nd}}$  values limited to data where both come from the same depth in the core, allowing us to test the two competing models presently underpinning most authigenic  $\varepsilon_{\text{Nd}}$  interpretations. We further present new downcore  $\varepsilon_{\text{Nd}}$  records from two scientific drill sites in the North Atlantic coupled with mineralogical data to take a deeper look at the implications of a bottom-up versus top-down model through time in context of local sedimentation and climate drivers as well as to provide a detailed regional intrabasinal comparison to complement the global compilation. We propose a new conceptual framework to understand the interplay between the three competing controls on the authigenic  $\varepsilon_{\text{Nd}}$  record proposed by the existing literature (bottom water, pore water, and sediment) which includes both top-down and bottom-up mechanisms. We then use this concept to frame our discussion around the degree to which authigenic  $\varepsilon_{\text{Nd}}$  is reflecting ocean circulation.

## 2. METHODS

### 2.1. Data compilation

A literature search and PANGAEA® database search identified sediment records containing paired authigenic and detrital  $\varepsilon_{\text{Nd}}$  measurements. We considered three types of authigenic records: foraminifera, sediment leaches, and fish teeth/debris. For detrital records, we considered both bulk sediment and residue analyses (Supplemental Table 1). Only data collected from the same sample (same core, same depth in core) were considered ‘paired’ and included in this compilation. This means that detrital data from a sample adjacent to a sample with authigenic data was not considered close enough and therefore not included in the compilation. Publications with less than 4 paired detrital-authigenic data points were not included. For the purpose of this compilation, we did not exclude any authigenic or detrital record based on methodology of the original study (Supplemental Table 1). The resulting compilation includes over 60 records from more than 20 publications for a total of over 870 paired detrital-authigenic data points. Data comes from every major ocean basin, the Caribbean, and the Mediterranean Sea (Supplemental Table 1).

This compilation is distinct to existing compilations (e.g. Jeandel et al., 2007; van de Flierdt et al., 2016; Tachikawa et al. 2017; Du et al., 2020; Robinson et al. 2021), which do not assemble exactly paired detrital-authigenic data, an essential requirement for examining the impacts of changing sediment composition on the neodymium isotope record. All marine data fulfilling our paired authigenic-detrital criteria was included regardless of depth, age, or proximity to the continental shelf. Recent work has shown that while shallow, near shore regions are more likely to have a very distinct neodymium isotope signature due to compositionally less mature sediments, the finer grained deep sea sediments are likely to have a larger benthic flux (Abbott et al., 2016; Abbott, 2019) highlighting the importance of including samples from a range of depositional settings to characterize general large scale trends and behavior. Furthermore, by not applying a depth, age, nor

location filter the inaccuracies introduced by over reliance on paleo depth and location reconstructions can be avoided.

We calculated the correlation coefficient using the CORREL function in excel ( $r$ , Eq. (1)) for the data set both with and without the end-member data from the Gulf of St. Lawrence (Casse et al., 2019) to test the sensitivity of the correlation to these extremely unradiogenic eastern Canadian values (Supplemental Fig. 1).

$$r(x,y) = \frac{\sum (x - \bar{x})(y - \bar{y})}{\sqrt{\sum (x - \bar{x})^2(y - \bar{y})^2}} \quad (1)$$

### 2.2. Sample preparation

Sediment samples were obtained from two International Ocean Discovery Program sites in the North Atlantic, ODP 1063 and IODP 1308 (Fig. 1). Sites were chosen to represent a region of the North Atlantic known to be impacted by the Heinrich Events of the last glaciation (1308, Blaser et al., 2019) and one with no reported influence of Heinrich events (1063, Roberts et al., 2010; Gutjahr and Lippold, 2011). Freeze dried sediment samples were hand milled with an agate mortar and pestle before processing. Approximately 150 mg of each sample from ODP 1063 and IODP 1308 was weighed out and transferred to acid cleaned Teflon beakers for hot plate digestion. An additional  $\sim 1$  g of samples from ODP 1063 was weighed out and transferred into acid cleaned 50 mL Falcon tubes for leaching to provide a direct comparison between the operationally defined authigenic component recovered (acid leachable) and the bulk sediment at the same core depth.

Bulk sediment digests were preferable over sediment residues because of the prevalence of detrital carbonates. Any attempt to pre-leach the sediments prior to digestion would have resulted in loss of this abundant detrital phase. Samples were digested using 4 mL trace metal grade hydrofluoric acid (48 wt%) and 2 mL distilled concentrated nitric acid in Teflon vials on a 150 °C hotplate. Samples were then refluxed in a mixture of  $\text{HClO}_4$ , HF and  $\text{HNO}_3$  on a 170 °C hotplate to break down resistant organic matter following the protocol of Nijenhuis and de Lange (2000). Following complete digestion, the REE fraction was isolated using AG50W-X8 spec resin with HF and HCl. Specifically, the columns were cleaned and conditioned prior to loading with 5 mL of 4 N HF, followed by 12 mL of 6 N HCl and finally 15 mL of a 2.5 N HCl and 0.1 N HF solution. Samples were then refluxed in a 2.5 N HCl and 0.1 N HF solution, centrifuged for 3 minutes then loaded onto the columns. Samples were then eluted through the column using 4 mL of a 2.5 N HCl and 0.1 N HF solution followed by 21.5 mL of 2.5 N HCl. Finally, the REE fraction was collected using 7 mL of 6 N HCl. Neodymium was further isolated using 1 mL Eichrom LN50-100 spec resin with 0.25 N HCl. Specifically, the columns were cleaned and conditioned with 15 mL of 0.25 M HCl prior to sample loading. Once loaded, samples were eluted using 1.25 mL of 0.25 M HCl. The neodymium cut was then collected in 4 mL of 0.25 M HCl. This was

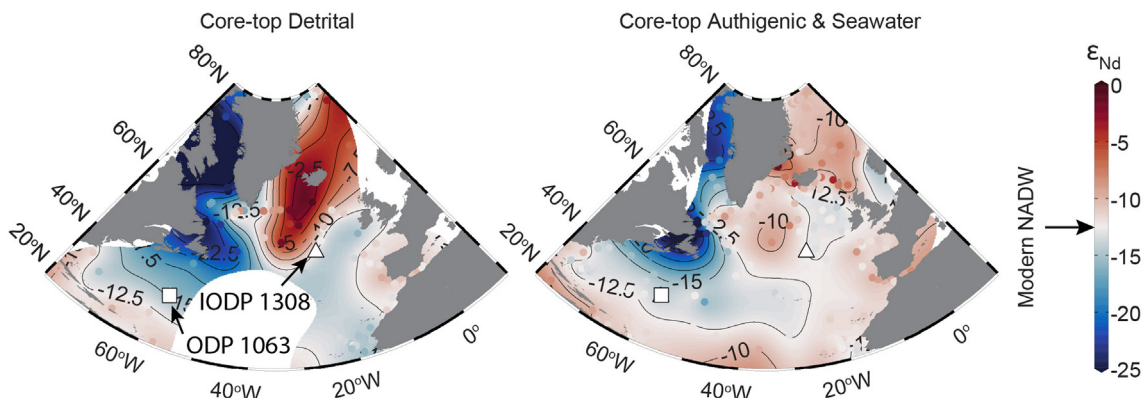


Fig. 1. Site locations of IODP Site 1308 (triangle) and ODP Site 1063 (square) overlain on authigenic  $\varepsilon_{\text{Nd}}$  (includes bottom water) and detrital  $\varepsilon_{\text{Nd}}$  maps of the modern North Atlantic (adapted from Du et al. 2020). The same positive correlation between authigenic  $\varepsilon_{\text{Nd}}$  versus detrital  $\varepsilon_{\text{Nd}}$  seen here is evident in our global compilation.

dried down and then dissolved in 3  $\mu\text{l}$  of 6 N distilled HCl to load on rhenium filaments for analyses on a Thermo Scientific Triton Thermal Ionization Mass Spectrometer (TIMS) at Macquarie University with a 1  $\mu\text{l}$  1 N HCl : 0.35 M  $\text{H}_3\text{PO}_4$  activator. Samples were analyzed using an evaporation filament current of 1200–1600 mA with a total Nd signal of 0.5–10 V. Analyses were collected in static mode with amplifier rotation in 4 blocks of 50 cycles each, with an integration time of 8.4 seconds per cycle. Ratios were normalized to  $^{146}\text{Nd}/^{144}\text{Nd} = 0.7219$  to correct for mass fractionation. Measured values for standards prepped and run the same as sediment digests were  $^{143}\text{Nd}/^{144}\text{Nd}$  BHVO-2 (average =  $0.512987 \pm 0.000021$ ,  $n = 4$ ) and NIST JMC 321 ( $0.511118 \pm 0.000005$ ,  $n = 1$ ) with long-term values for the facility being  $^{143}\text{Nd}/^{144}\text{Nd}$  BHVO-2 (average =  $0.512973 \pm 0.000012$ ,  $n = 71$ ) and NIST JMC 321 ( $0.511 \pm 0.000017$ ).

Sediments from ODP 1063 were leached using a buffered acetic acid solution (after Abbott et al., 2016). Briefly, 10 mL of milli-Q water was added to each Falcon Tube with approximately 1 g of dried sediment and the sample was shaken by hand and allowed to sit for five minutes. The mixture was then centrifuged at 4000 rpm for 15 minutes and the overlying solution decanted. This was repeated for a total of 3 times. The acid leachable fraction was then targeted by adding 10 ml of buffered acetic acid solution (0.5 M sodium acetate, 2.5 M glacial acetic acid in milliQ, pH 3.5–4) to each sample. The samples were shaken for two hours and then centrifuged at 4000 rpm for 20 minutes. Following centrifugation, 8 mL of the solution was pipetted into acid-cleaned Teflon and dried completely at 120 °C on a hotplate overnight. This aliquot was then refluxed in 2 mL quartz distilled concentrated  $\text{HNO}_3$  at 120 °C, dried, and then refluxed in a mixture of  $\text{HClO}_4$ , HF and  $\text{HNO}_3$  was added and fluxed at 160 °C following the same protocol as above (Nijenhuis and de Lange, 2000). Samples were then dried completely, refluxed in 2 ml of 2.5 N HCl and 0.1 N HF and separated using the sample column chromatography technique applied to the bulk digest.

Bulk mineralogy of representative samples from both sites was determined by X-ray diffractometry (XRD).

Freeze-dried samples were homogenised in an agate mortar and pestle, before back-loading into 25 mm internal diameter stainless steel sample holders. X-ray powder diffraction patterns spanning 5 to 90° 2 $\theta$  were collected using a PANalytical Aeris benchtop XRD instrument (0.02° step size, Cu-radiation source with 40 kV generator voltage and 15 mA tube current, 1/8 inch divergence slits and 23 mm beam mask). Diffraction patterns were interpreted using Panalytical HighscorePlus software with the ICSD database for phase identification. Whole-pattern clustering in Highscore Plus facilitated the identification of lithological or compositional groupings within the samples.

SEM images and mineral maps were collected from eight samples following previously published methods (Supplemental Table 2; Abbott et al., 2019, Frank et al., 2020). Briefly, we used scanning electron microscope (SEM) analysis on an FEI Teneo LoVac field emission SEM equipped with dual Bruker XFlash Series 6 energy dispersive X-ray spectroscopy (EDS) detectors to produce high resolution mineral maps of each sediment sample. Freeze dried sediment samples were mounted in epoxy and then polished. We removed any surface damage or smearing to these resin mounts caused by the mechanical polishing using a Hitachi IM4000 Argon Ion Mill (10° beam incident angle, 5 kV accelerating voltage, 30 minutes with continuous sample rotation). Samples were carbon-coated before placement in the SEM. Backscatter electron (BSE) image tilesets (~600 nm pixel resolution for overview tilesets, ~70 nm pixel resolution for selected regions of interest) and EDS spectra (1.5  $\mu\text{m}$  step size, 8 ms dwell time) were collected sequentially using the FEI Maps Mineralogy software followed by classification of the individual EDS spectra using the FEI Nanomin software of smaller, representative regions of interest chosen after inspection of the BSE overview images (Haberlah et al., 2015). Mineral identification in the Nanomin® software is achieved by comparing EDS spectra collected in the mapped area against reference spectra collected on known mineral standards. Unlike other SEM-based mineral mapping techniques (e.g. QEMSCAN), the Nanomin mineral classification system can deconvolve mixed X-ray spectra and assign up to three min-

erals per analyzed spot. This is a critical requirement for the correct interpretation of the mixed phase X-ray spectra characteristic of heterogeneous fine-grained sediments, where the X-ray generating electron interaction volume is commonly larger than the grain size. This results in accuracy and precision comparable to quantitative XRD analysis (Rafiei et al., 2020).

### 2.3. Age Models

A linear age model based on the data provided in Hodell et al. (2008) was used for ODP Site 1308. Specifically, we used the ages from 0.68 to 2.01 mcd, resulting in the age (ky) = 18.78 (depth in meters) + 0.3649. Both our new detrital data and the existing sediment leach record from Blaser et al. (2019) were plotted using this approach. Identification of Heinrich Events in nearby site 980 (Crocker et al., 2016) was also used in identification of events older than those reported by Blaser et al. (2019). For IODP Site 1063, we used a linear age depth model based on Roberts et al. (2010) and identified two distinct age-depth relationships breaking at 1.42 mcd. For all samples above 1.42 mcd, we calculated the age as age (ky) = 0.108 (depth in meters) – 0.2396 and for all samples below 1.42 mcd we calculated the age as age (ky) = 0.018 (depth in meters) + 11.824.

## 3. RESULTS

### 3.1. Global Compilation

Our global compilation demonstrates a strong (correlation coefficient = 0.86; n = 871) overall correlation between authigenic archives and detrital phases (Fig. 2; Table 1). Without the Gulf of St. Lawrence dataset the correlation coefficient is still 0.85 (n = 861; Supplemental Fig. 1). Even considered individually, each type of authigenic record still displays significant correlation with the corresponding detrital material (Table 1). However, the sediment leachate  $\varepsilon_{\text{Nd}}$  records do have a lower correlation coefficient with the detrital  $\varepsilon_{\text{Nd}}$  values than the fish teeth/debris or foraminifera datasets, likely a result of the range of leaching protocols employed (Table 1; Supplemental Table 1) and the potential for leaches to target unintentional phases including variably abundant trace phases that may have Nd isotopic compositions that differ significantly from the bulk (e.g. Wilson et al., 2012; Abbott et al., 2016; McKinley et al., 2019). The fish teeth/debris appears to separate into two populations, one with an  $\varepsilon_{\text{Nd}}$  similar to detrital and one with a more radiogenic  $\varepsilon_{\text{Nd}}$  signature than the detrital, but both populations are highly correlated to the detrital component (Fig. 1d). This compilation broadly shows more negative  $\varepsilon_{\text{Nd}}$  values for both detrital and authigenic phases in the North Atlantic that become progressively more positive in the Indian and Arctic basins with the most positive values observed in the North Pacific but there is significant overlap in the  $\varepsilon_{\text{Nd}}$  range between basins (Fig. 1; e.g. Groussset et al., 1988; Jeandel et al., 2007; Du et al., 2020; Robinson et al., 2021).

### 3.2. Neodymium Isotopes from ODP 1063 and IODP 1308

The  $\varepsilon_{\text{Nd}}$  of the bulk sediments from IODP 1308 spans a larger range than  $\varepsilon_{\text{Nd}}$  of the bulk sediments from ODP Site 1063. Specifically, bulk sediment  $\varepsilon_{\text{Nd}}$  ranged between  $-12.0 \pm 0.1$  and  $-23.2 \pm 0.1$  at IODP Site 1308 and between  $-11.7 \pm 0.1$  and  $-16.0 \pm 0.1$  at ODP Site 1063 (Fig. 3; Fig. 4; Supplemental Table 3). The largest negative excursion in the bulk sediments at Site 1308 occurred at 52 kyr (Heinrich Event 5, Fig. 5), with additional negative excursions at 38.9 kyr (coincident with Heinrich Event 4; Crocker et al., 2016), 23.8 kyr (Heinrich Event 2), and 17.3 kyr (Heinrich Event 1). No sediment samples were available for Heinrich Event 3 from site 1308. Sediments at Site 1063 were consistently  $\sim -12$  throughout the Last Glacial Maximum with the only large negative excursion ( $\varepsilon_{\text{Nd}} - 16$ ) in the last 25 kyrs beginning following the onset of the Holocene (10.7 kyr) with a subsequent gradual rebound towards more radiogenic values in modern sediments (Fig. 4; Supplemental Table 3). The acid leachable fraction (sediment leach) from Site ODP 1063 ranged between  $-10.2 \pm 0.1$  and  $-13.3 \pm 0.1$  (Fig. 4; Supplemental Table 3). While following the same general trend, the magnitude of changes in the  $\varepsilon_{\text{Nd}}$  of the acid leachable fraction was smaller at Site 1063 than the magnitude of the changes observed in the  $\varepsilon_{\text{Nd}}$  of the bulk sediment (Fig. 5). The acid leachable fraction ( $\varepsilon_{\text{Nd}} - 11$ ) was generally more radiogenic than the bulk sediment and had negative excursions at 24 kyr ( $\varepsilon_{\text{Nd}} - 12.8$ ), coincident with an abrupt slow down in Atlantic Meridional Overturning Circulation (Fig. 4), and from 14 to 12 kyr ( $\varepsilon_{\text{Nd}} - 13.3, -12.9$ ), coincident with the Bølling Allerød and Younger Dryas (Ng et al., 2018).

### 3.3. Mineralogical Properties

#### 3.3.1. IODP 1308

Bulk powder XRD analysis and SEM-EDS mineral mapping of Site 1308 materials reveals a clear compositional shift with the onset of carbonate ooze deposition in the Holocene ( $\sim 11$  kyr). Whole-pattern cluster analysis of X-ray diffractograms identifies two classes of muds prior to this, punctuated by an influx of coarse IRD during Heinrich Events 1, 2, 4 and 5 (Fig. 5; Supplemental Table 3): 1) mixed calcareous-clastic muds, containing  $> 20\%$  calcite (foraminifera and coccolithophore remains) and minor detrital dolomite, in addition to feldspar, quartz, illite and chlorite and 2) carbonate-lean clastic muds, containing  $< 15\%$  calcite and dolomite, and commensurately higher abundances of feldspar, quartz, illite and chlorite (Fig. 3). Heinrich Events 1 and 2 (as identified by Hodell et al., 2017; Blaser et al., 2019) are compositionally distinct and contain abundant IRD including sand to silt size igneous and metasedimentary lithic grains, quartz, feldspar, as well as abundant detrital dolomite and calcite grains, in an illite and chlorite clay rich matrix. Heinrich Events 4 and 5, by contrast, are compositionally more similar to the carbonate-lean clastic sediments that are characteristic of this site for the majority of the last glacial interval. This is likely because of the dominance of feldspar

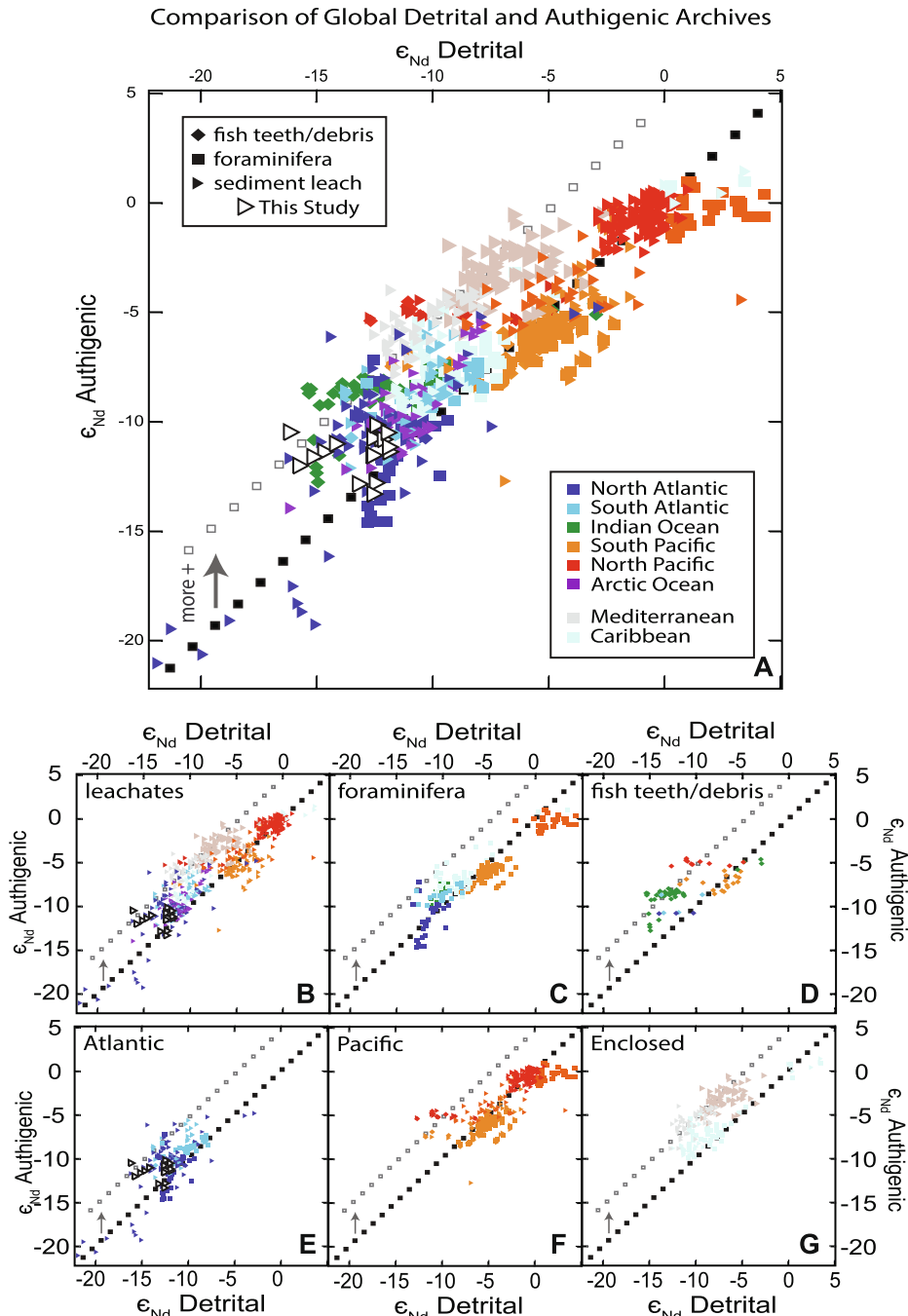


Fig. 2. Global compilation of paired authigenic  $\epsilon_{\text{Nd}}$  and detrital  $\epsilon_{\text{Nd}}$  records (A). The strong linear correlation (correlation coefficient = 0.86,  $n = 871$ ) across all basins and the various archive types suggests widespread influence of lithogenically sourced neodymium, likely during early diagenesis (full list of data sources in SI). A 1 to 1 relationship is illustrated by the dotted line (black squares). The open squares represent the same slope but offset with authigenic records more radiogenic than their corresponding detrital record. This authigenic shift towards radiogenic values is most evident in more enclosed basins receiving volcanoclastic detritus, such as the Mediterranean (grey) and Caribbean (turquoise). Authigenic archives include sediment leaches (triangles, and B), foraminifera (square, and C), and fish debris (diamonds, and D), from the North Atlantic (dark blue), South Atlantic (light blue), Indian (green), South Pacific (orange), North Pacific (red), and Arctic (purple) oceans. For comparison purposes, we also present the data by location showing the Atlantic (E), Pacific (F), and enclosed basins (G) as separate panels. The similarity in correlation with detrital between all commonly reported authigenic archive types (leachate, foraminifera, or fish debris) demonstrates this relationship is not simply an artifact of sediment leaching protocols. (For interpretation of the references to colour in this figure legend, the reader is referred to the web version of this article.)

Table 1

Dataset sample size and correlation coefficient.

Dataset	n	Correlation Coefficient
All Authigenic	871	0.86
All w/out Casse	861	0.85
Fish Teeth/Debris	67	0.92
Foraminifera	237	0.87
Sediment Leachates	567	0.63

as well as large igneous and metasedimentary IRD accompanied by relatively lower quantities of detrital calcite and dolomite.

### 3.3.2. ODP 1063

Bulk powder XRD analysis and SEM-EDS mineral mapping identifies a major lithological transition from a carbonate-lean mud with abundant quartz and feldspar silt prior to  $\sim 14.9$  kyr to a calcareous mud from  $\sim 12.3$  kyr (Supplemental Table 3). The carbonate lean muds are dominantly composed of illite, smectite, and chlorite clays as well as abundant quartz, feldspar, muscovite, and lithic silt grains up to 50  $\mu\text{m}$  in size, with SEM analysis further identifying abundant biogenic siliceous material (Fig. 3). Calcite ( $\ll 10\%$ ) is mainly present as foraminiferal tests, in addition to ubiquitous detrital dolomite grains ( $\sim 1\text{--}2\%$ ). The calcareous mud has a similar mineral assemblage but contains less biogenic silica and a higher proportion of foraminiferal

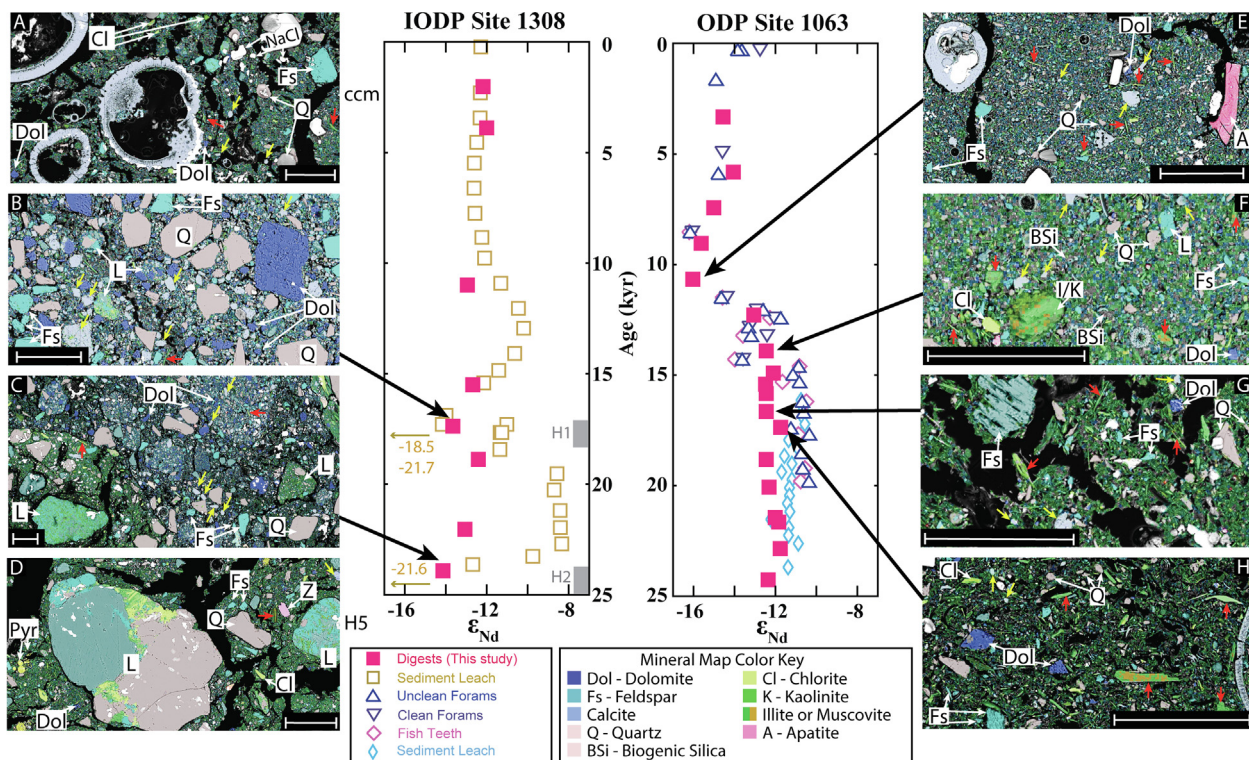


Fig. 3. Downcore  $\epsilon_{\text{Nd}}$  and mineralogical variation for IODP Site 1308 and ODP Site 1063. Bulk  $\epsilon_{\text{Nd}}$  (this study, solid pink squares) is shown compared to existing authigenic  $\epsilon_{\text{Nd}}$  records including sediment leach (weak hydroxylamine hydrochloride leach without decarbonation brown open squares Blaser et al. 2019; strong hydroxylamine hydrochloride leach without decarbonation blue diamonds Gutjahr and Lippold, 2011), foraminifera (open blue triangles, Roberts et al. 2010), and fish teeth (open pink diamonds, Roberts et al. 2010). Authigenic and bulk sediment neodymium records co-vary, consistent with the global trend identified in Fig. 3. Panels show mineralogical characteristics obtained by SEM-based mineral mapping of select down core samples. Quartz (Q, pink), Feldspar (fs), detrital Calcite (yellow arrow), Micas (red arrow), Dolomite (Dol, periwinkle), clay minerals (green), salts (bright white), lithic grains (L, multi color), and apatite (A, bright pink). Foraminifera and other biogenic calcite present but not labeled. All scale bars represent 100  $\mu\text{m}$ . **a)** mixed calcareous and clastic mud (ccm); Supplemental Table 3) at IODP 1308 are comprised of detrital clays, silts and biogenic carbonates **b)** Heinrich event 1 (H1) contains IRD including quartz, dolomite, calcite, and lithic fragments including some metasedimentary grains. The fine-grained matrix comprises detrital clays, biogenic carbonates, and detrital carbonates. Calcite and dolomite are the most abundant IRD constituents in the silt to fine sand size range **c)** Heinrich event 2 (H2) also contains larger IRD including quartz and lithic grains. Calcite and dolomite are the most abundant IRD constituents in the silt to fine sand size range. The matrix is dominantly detrital carbonates and clays, some biogenic carbonates **d)** Heinrich event 5 (H5) shows abundant large metasedimentary lithic clasts corresponding to a strong unradiogenic  $\epsilon_{\text{Nd}}$  signature **e)** Deglacial interval is a calcareous mud with detrital clays, biogenic silica, quartz, and some larger feldspar and apatite grains **f)** Glacial sediments with mainly fine grained matrix of detrital clays and biogenic opal with some detrital carbonates **g)** Glacial, similar to (f) with a few larger detrital calcites and feldspars visible **h)** Glacial, similar to (f) with a few larger mica and dolomite grains visible. Fig. 4 provides a further in depth examination of Site 1063 including sediment leach records not shown here. (For interpretation of the references to colour in this figure legend, the reader is referred to the web version of this article.)

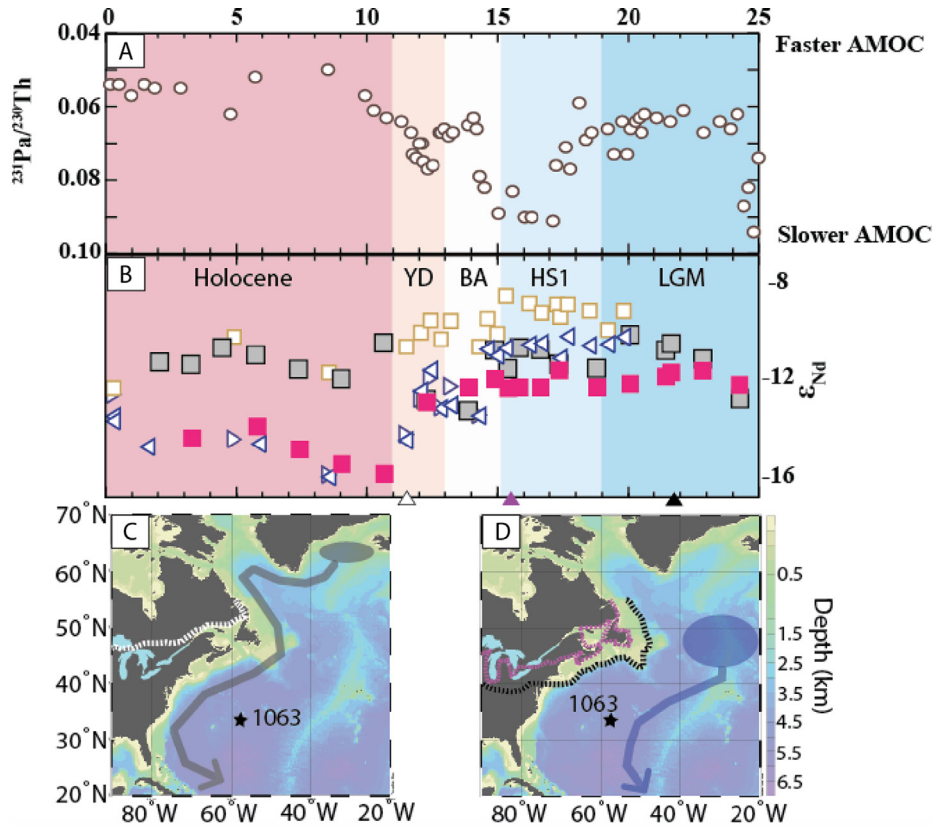


Fig. 4. Changes in ocean circulation, ice extent and resulting  $\varepsilon_{\text{Nd}}$  record at Bermuda Rise ODP site 1063. **A)** Record of Atlantic Meridional Overturning Circulation strength as indicated by  $^{231}\text{Pa}/^{230}\text{Th}$  (from Ng et al., 2018); **B)** Bulk sediment  $\varepsilon_{\text{Nd}}$  (pink squares, this study); bulk sediment leach  $\varepsilon_{\text{Nd}}$  (grey square, this study); decarbonated sediment leach  $\varepsilon_{\text{Nd}}$  (brown open squares, Roberts et al., 2010), and foraminifera  $\varepsilon_{\text{Nd}}$  (triangles, Roberts et al., 2010) for the last 25 kyr from site 1063. Triangles on the bottom  $\times$  axis indicate timing of ice margin extent shown in **(C)** and **(D)**. **C)** Location of site 1063 (black star) with simplified schematic of the location of Holocene deep water formation and deep to intermediate currents after Seidov and Maslin (1999) in grey and approximate ice extent at 11.5 kyr (white hashed line) after Margold et al., 2018. **D)** Location of site 1063 (black star) with simplified schematic of the location of deep water formation and deep to intermediate currents during the Last Glacial Maximum after Seidov and Maslin (1999) in blue and approximate ice extent at 21.8 (black hashed line) and 15.5 kyr (purple hashed line) after Margold et al., 2018. Maps for **(C)** and **(D)** created using Ocean Data View (Schlitzer, R., Ocean Data View, <http://odv.awi.de>, 2016).

and coccolithophore calcite, contributing to carbonate abundances mostly > 25% wt, as well as silt size material that is notably less abundant and finer grained (<20  $\mu\text{m}$ ). Sample D1 H1 130–132 (~13.9 kyr) is transitional to the two, containing ~ 15% calcite and returns the most radiogenic leach value  $\varepsilon_{\text{Nd}}$  measured at this site ( $\varepsilon_{\text{Nd}} = -13.3$ ; Supplemental Table 3).

### 3.4. Literature-based conceptual framework

Finally, we synthesized existing literature to design a new conceptual framework to understand the interplay between the major potential controls on the authigenic  $\varepsilon_{\text{Nd}}$  record from both the traditional top-down and more recently proposed bottom-up models for neodymium cycling in the ocean (Fig. 6). Most paleoclimate studies using authigenic  $\varepsilon_{\text{Nd}}$  ocean circulation reconstructions assume that these authigenic records reflect bottom water values (e.g. Rutberg et al., 2000; Frank, 2002; Scher and Martin, 2004; Gutjahr and Lippold, 2011; Böhm et al.,

2015; Huck et al., 2016; Basak et al., 2018; Blaser et al., 2019). In this top-down understanding of the neodymium cycle in the ocean, the authigenic  $\varepsilon_{\text{Nd}}$  is controlled by the  $\varepsilon_{\text{Nd}}$  of bottom water; this forms the basis for our first scenario (Fig. 6a). The alternative, described by the bottom-up model (e.g. Haley et al., 2017), is that the reactive phases of the sediment exert control over bottom water  $\varepsilon_{\text{Nd}}$  via the pore water (benthic flux, Abbott et al., 2015b). However, there are two ways within this model for the sediments to influence the authigenic record so we split the bottom-up processes into two separate scenarios. The sediments can either influence the authigenic record via the benthic flux's impact on the bottom water  $\varepsilon_{\text{Nd}}$  (Fig. 6b, e.g. Abbott et al., 2015b; Haley et al., 2017) or directly in the sediment column during early diagenesis (Fig. 6c; e.g. Abbott et al., 2019; Skinner et al., 2019) forming our scenario 2 and scenario 3 respectively. We stress that a true separation between scenario 2 and 3 can only occur if the  $\varepsilon_{\text{Nd}}$  of the authigenic phase is determined before burial (e.g. in the bottom water) or if there is no local benthic flux. However,

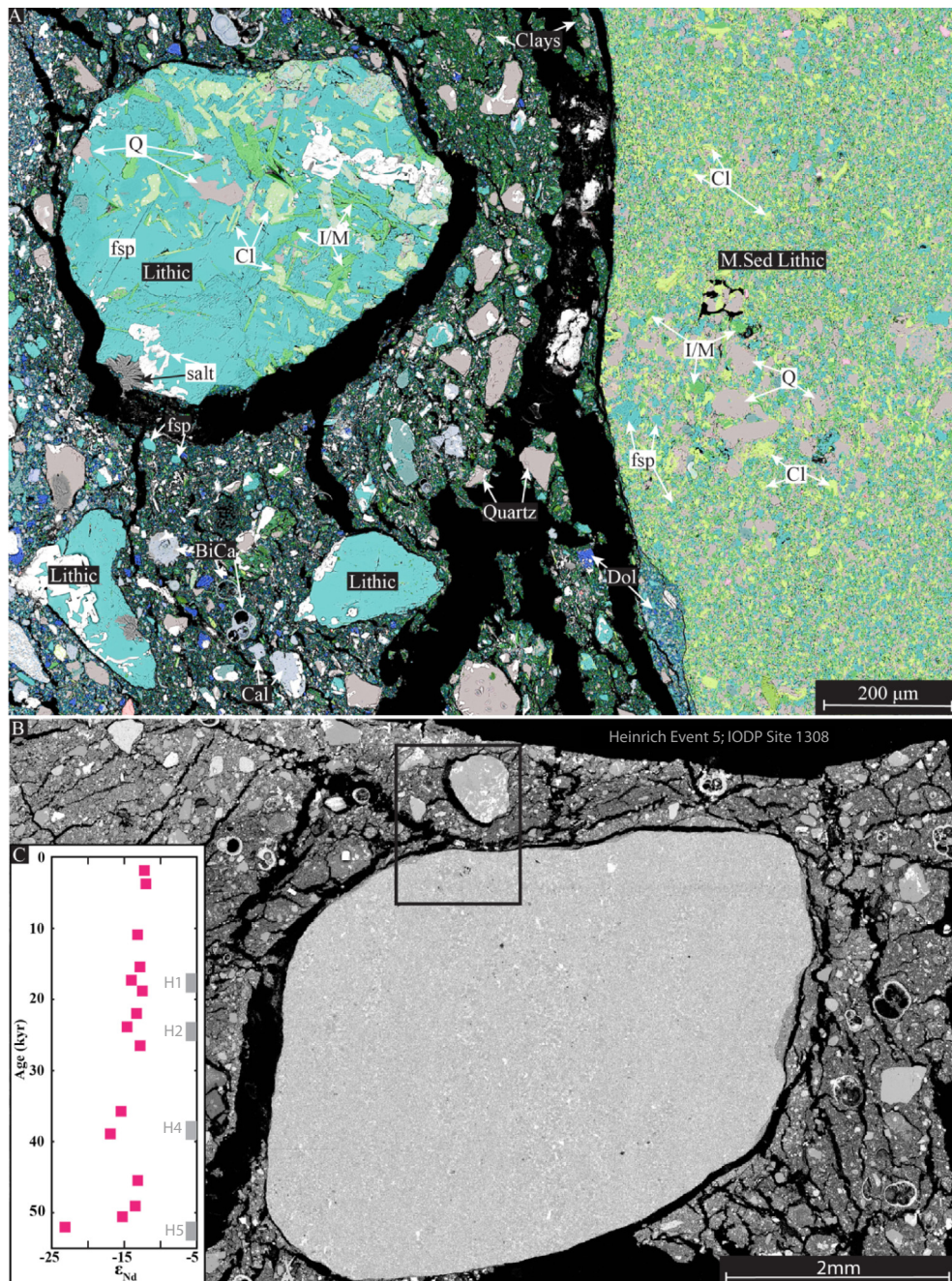


Fig. 5. Mineral map (A) and backscatter electron image (BSE, B) of IODP Site 1308 Heinrich Event 4. The area from which the mineral map is taken is outlined with a black box on the BSE image (B). Note that the mineral map (A) is at a 90° rotation from the BSE image (B). Sediments corresponding to Heinrich Event 5 had the largest abundance of lithics including large metasedimentary clasts (diameter > 400  $\mu\text{m}$ ). Also visible is quartz, detrital calcites (Cal), dolomite (Dol), and feldspars (fsp). Some biogenic calcite (BiCa) is present although overall, the sparse occurrence of foraminifera is consistent with observations from Heinrich Events 1 and 2. The same color legend as in the main text is used in (A). Inset (C) shows full profile of bulk sediment  $\epsilon_{\text{Nd}}$  for IODP 1308 extending through Heinrich Event 5.

imposing a separation between the two scenarios allows us to demonstrate how the resulting  $\epsilon_{\text{Nd}}$  of the authigenic phases from the two processes differ and highlights the importance of when the authigenic phase acquires its isotopic signature. Therefore, we consider these three scenarios as analogous to the ‘end-members’ in end-member

mixing in that each scenario isolates a single process and looks at the results if that process is completely dominant at a given site and time. However, we consider it likely that at any given site more than one of these processes may be important and therefore two scenarios may be simultaneously applicable. We describe each end-member scenario

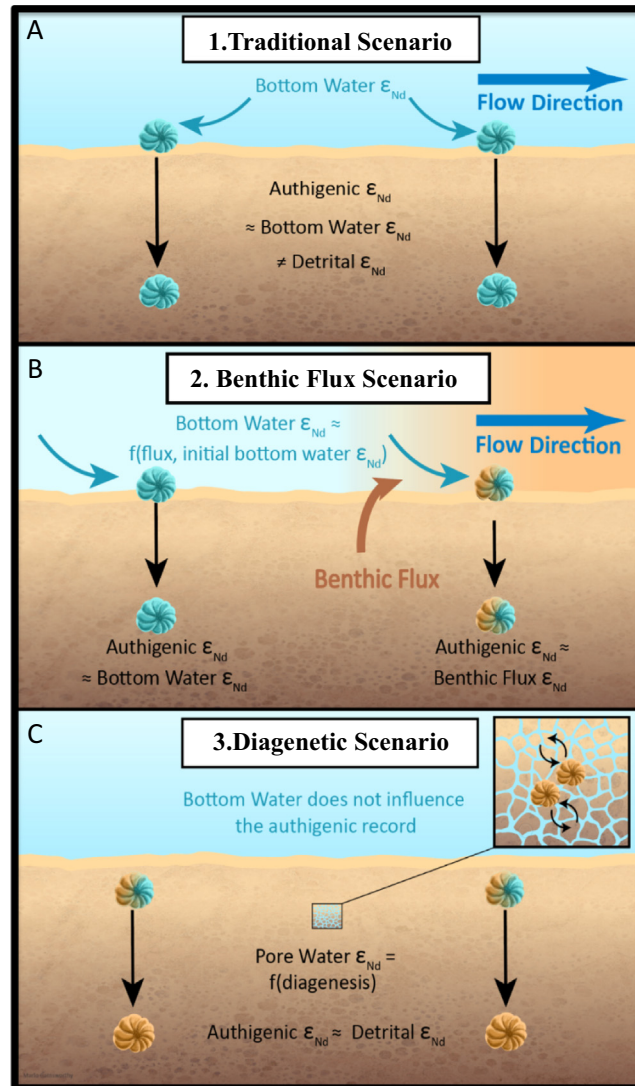


Fig. 6. Framework for interpreting authigenic  $\epsilon_{\text{Nd}}$  records, with three end-member scenarios; 1) ‘Traditional’ Scenario: authigenic  $\epsilon_{\text{Nd}}$  is strictly a record of bottom water  $\epsilon_{\text{Nd}}$ , detrital  $\epsilon_{\text{Nd}}$  does not influence either, 2) Benthic Flux Scenario: detrital  $\epsilon_{\text{Nd}}$  can alter the bottom water  $\epsilon_{\text{Nd}}$  through the benthic flux, and the authigenic  $\epsilon_{\text{Nd}}$  then records that altered bottom water  $\epsilon_{\text{Nd}}$  [function of circulation speed, exposure time, distance traveled, magnitude and character of benthic flux], and 3) Diagenetic Scenario: bottom water  $\epsilon_{\text{Nd}}$  is not preserved in the authigenic  $\epsilon_{\text{Nd}}$  record, instead authigenic  $\epsilon_{\text{Nd}}$  is strictly a function of the composition and reactivity of the detrital components, exchanging via pore water. The relative importance of each scenario may change both temporally and spatially. Artwork by Marlo Garnsworthy, Wordy Bird Studios.

in detail below, including the expected impact on the authigenic  $\epsilon_{\text{Nd}}$  record.

In the **traditional scenario (1)**,  $\epsilon_{\text{Nd}}$  behaves conservatively in bottom water and is only changed through water mass mixing. This means that the bottom water  $\epsilon_{\text{Nd}}$  can act as a tracer for water mass movement because of the heterogeneity of continental  $\epsilon_{\text{Nd}}$  around the globe, therefore revealing the water mass’s origin based on the neodymium fingerprint (e.g. Frank, 2002). Furthermore, in this scenario the bottom water  $\epsilon_{\text{Nd}}$  sets the authigenic  $\epsilon_{\text{Nd}}$ , and this authigenic  $\epsilon_{\text{Nd}}$  remains unaltered during diagenesis (Fig. 6a). The pore water  $\epsilon_{\text{Nd}}$  is inherited from the bottom water  $\epsilon_{\text{Nd}}$  and there is no active sediment-fluid interaction under ambient conditions. Without reactive sediment

phases, the sediment acts only as a sink for Nd and there is no benthic source at these locations. Because the authigenic  $\epsilon_{\text{Nd}}$  is only dependent on the overlying water mass’s origin in this scenario, the authigenic  $\epsilon_{\text{Nd}}$  can be entirely decoupled from the local detrital  $\epsilon_{\text{Nd}}$  record. This could explain why GEOTRACES data from 70°N to 20°S in the North Atlantic today demonstrates a nearly constant modern bottom water  $\epsilon_{\text{Nd}}$  with only slight deviations from -13 to -11 near the southern tip of Greenland and again at the southern end of the profile (Lambelot et al., 2016) yet over the same transect we see a nearly 20  $\epsilon$  change in detrital  $\epsilon_{\text{Nd}}$  (e.g. Du et al., 2020; Robinson et al., 2021; Fig. 1a). In this example, if scenario 1 is dominant we expect that the authigenic  $\epsilon_{\text{Nd}}$  should remain equal to bottom water (-13)

irrespective of detrital composition and only change upon the intrusion of a different water mass into the region. In summary, under scenario 1 changes in the authigenic  $\varepsilon_{\text{Nd}}$  record reflect changes in ocean circulation (e.g. Frank, 2002; Huck et al., 2016; Basak et al., 2018; Blaser et al., 2019) and bottom water  $\varepsilon_{\text{Nd}}$  and detrital  $\varepsilon_{\text{Nd}}$  can be de-coupled as seen in the North Atlantic today.

In the **benthic flux scenario (2)**, the authigenic  $\varepsilon_{\text{Nd}}$  is still determined by the  $\varepsilon_{\text{Nd}}$  of the bottom water (as in scenario 1), however the bottom water itself is altered by a benthic flux (Fig. 6b; non-conservative behavior of  $\varepsilon_{\text{Nd}}$  in the bottom water after Abbott et al., 2015b; Abbott, 2019). The benthic flux represents the elements introduced into the bottom water via a diffusive flux from higher concentrations in the pore water to lower concentrations in the bottom water either at the study location or earlier along the water mass's flow path (e.g. Haley et al., 2004; Abbott et al., 2015b; Haley et al., 2017). In this scenario the resulting authigenic  $\varepsilon_{\text{Nd}}$  record is a function of the magnitude and isotopic nature of the benthic flux and the exposure time of a water mass to that flux. The bottom water is continually influenced by the sediments as it moves, making the bottom water  $\varepsilon_{\text{Nd}}$  at any given location also a function of the water mass's flow path and speed (inverse to exposure time, e.g. Abbott et al., 2015b; Haley et al. 2017). Given that this scenario assumes that authigenic phase  $\varepsilon_{\text{Nd}}$  is set by the bottom water  $\varepsilon_{\text{Nd}}$  and not altered in the sediment column (notwithstanding the reactive sediments needed to drive a local benthic flux), the degree of coupling between authigenic  $\varepsilon_{\text{Nd}}$  and detrital  $\varepsilon_{\text{Nd}}$  is going to be a function of the local benthic flux (magnitude and  $\varepsilon_{\text{Nd}}$ ) as well as the flow path. That is, if the local benthic flux (with an  $\varepsilon_{\text{Nd}}$  approximated by that site's detrital  $\varepsilon_{\text{Nd}}$ ) is large enough or circulation is slow enough for the influence of the local benthic flux to be the dominant control on the bottom water  $\varepsilon_{\text{Nd}}$  at that site we expect a coupling between authigenic  $\varepsilon_{\text{Nd}}$  and detrital  $\varepsilon_{\text{Nd}}$ . However, if circulation is strong or there is a weak local benthic flux, decoupling between authigenic  $\varepsilon_{\text{Nd}}$  and detrital  $\varepsilon_{\text{Nd}}$  is possible as the bottom water  $\varepsilon_{\text{Nd}}$  will be an integrated signature of the different inputs along its flow path, as a 'memory' of where the water mass had been previously. This idea of circulation outweighing the local benthic flux could also be consistent with the observed modern North Atlantic  $\varepsilon_{\text{Nd}}$  distribution discussed above. Overall, in the benthic flux scenario the degree of decoupling should be, at least in part, controlled by the magnitude of the benthic flux at a given location. In summary, in regions with a locally high benthic flux (exaggerated by sluggish circulation) we expect the bottom water  $\varepsilon_{\text{Nd}}$  to be altered to be more similar to the local sedimentary  $\varepsilon_{\text{Nd}}$  (strongly coupled) whereas in regions of no local benthic flux or very low local benthic flux (exaggerated by strong circulation) the bottom water would have a longer lasting 'memory' of upstream  $\varepsilon_{\text{Nd}}$  inputs (decoupled; e.g. Abbott et al., 2016; Haley et al., 2017; Tachikawa et al., 2017).

In our **diagenetic scenario (3)**, authigenic  $\varepsilon_{\text{Nd}}$  is only dependent on the surrounding sediments and does not record bottom water  $\varepsilon_{\text{Nd}}$  (Fig. 6c). Here we neglect the isotopic composition of bottom water (i.e. pore water at time = 0), consistent with observations that the concentra-

tion of Nd in bottom water is often 1 to 2 orders of magnitude lower than the Nd concentration of pore water, which itself only contains < 0.001% of the total Nd reservoir in the sediments (e.g. Haley et al., 2004; Abbott et al., 2015a, 2016; Du et al., 2016), making bottom water composition inconsequential in a sediment-dominated system. This scenario predicts that the authigenic  $\varepsilon_{\text{Nd}}$  record is determined entirely within the sediment column, meaning the resulting authigenic  $\varepsilon_{\text{Nd}}$  will be a function of the reactivity and  $\varepsilon_{\text{Nd}}$  of sediment components (a reactivity-weighted average  $\varepsilon_{\text{Nd}}$ ) so there should be a strong coupling between authigenic  $\varepsilon_{\text{Nd}}$  and detrital  $\varepsilon_{\text{Nd}}$ . Importantly, while we do not consider bottom water in terms of an influence on the authigenic record in this scenario, the bottom water itself is likely highly altered as a reactive sediment column can be expected to have elevated Nd concentrations in the pore water and thus a high resulting benthic flux. The distinction in scenario 3 is that while benthic flux is very much present, the authigenic phase acquires its Nd isotopic signature in the sediment column restricting the detrital influence to the local sediment composition and removing the 'memory' effect possible when the authigenic signature is determined by the bottom water. Additionally, because the pore water  $\varepsilon_{\text{Nd}}$  is driven by the reactive sediment components, we can use existing pore water  $\varepsilon_{\text{Nd}}$  measurements to understand how quickly this evolution of isotope values towards sediment values can occur. These  $\varepsilon_{\text{Nd}}$  pore water profiles demonstrate that by 1 cm sediment depth the  $\varepsilon_{\text{Nd}}$  of the pore water is already more closely resembling the value recorded in deeper pore water (8–12 cm) than that of overlying bottom water (highest resolution currently available, Abbott et al., 2015b). This demonstrates that the early diagenetic processes driving this scenario occur without significant burial. Therefore, the  $\varepsilon_{\text{Nd}}$  of authigenic phases, even in the upper cm of the sediment column, can already be reflective of the sedimentary  $\varepsilon_{\text{Nd}}$ . Notably, this scenario permits authigenic phases to continue to change throughout diagenesis through dissolution-precipitation cycles, secondary mineral phases growth, and the replacement of primary phases (e.g. Abbott et al., 2019; Skinner et al., 2019), whereas scenarios 1 and 2 assume that the authigenic phase maintains the bottom water signature through time.

Scenario 2 and scenario 3 are closely related because both require active sediment-fluid interactions during early diagenesis and, as seen above, both may result in coupling between authigenic  $\varepsilon_{\text{Nd}}$  and detrital  $\varepsilon_{\text{Nd}}$ . The magnitude of a benthic flux (scenario 2) will be determined by sediment reactivity and the amount of opportunity for interactions between solid and fluid phases such as exposure time, sedimentation rate, and grain size (Wilson et al., 2012; Pearce et al., 2013; Roberts and Piotrowski, 2015; Abbott et al., 2016; Du et al., 2016; Homoky et al., 2016; Howe et al., 2016; Haley et al., 2017; Blaser et al., 2019; Abbott et al., 2019; Vogt-Vincent et al., 2020; Jaume-Sequí et al., 2021). These solid–fluid interactions driving the benthic flux via the pore water in scenario 2 are the same interactions determining the pore water in which authigenic phases form and alter in scenario 3. We expect scenario 2 and 3 to produce the most similar result in regions with high benthic flux (i.e. bottom water  $\varepsilon_{\text{Nd}} \approx$  pore water  $\varepsilon_{\text{Nd}} \approx$  sediment  $\varepsilon_{\text{Nd}}$ )

due to increased sediment–water interactions (presence of reactive detritus) resulting in a tight correlation between the authigenic and detrital  $\varepsilon_{\text{Nd}}$  signatures under both scenarios. In these regions the reactive sediment will determine the pore water  $\varepsilon_{\text{Nd}}$ , which in turn will alter the bottom water to resemble the pore water  $\varepsilon_{\text{Nd}}$  via the benthic flux. This means that regardless of whether the authigenic  $\varepsilon_{\text{Nd}}$  reflects altered bottom water (scenario 2) or pore water (scenario 3), the authigenic  $\varepsilon_{\text{Nd}}$  will ultimately be recording a bulk signature weighted towards more reactive sediment components (e.g. Abbott et al., 2016; Du et al., 2016; Abbott et al., 2019). In contrast, the result of scenario 2 on the other extreme in regions of lower benthic flux or strong circulation (not enough reactive detritus to significantly influence bottom water  $\varepsilon_{\text{Nd}}$ ), the expected decoupling between authigenic  $\varepsilon_{\text{Nd}}$  and detrital  $\varepsilon_{\text{Nd}}$  could either approach scenario 1 (no significant benthic influence) or be the result of a strong ‘memory’ of the integrated benthic inputs along the water mass’ preceding flow path.

Similarly, both scenarios 2 and 3 are complicated in situations when the sediment contains minor, but isotopically unique, components that are highly reactive (e.g. ‘cryptic phase’ of Abbott et al., 2016). This situation can cause the bulk sediment  $\varepsilon_{\text{Nd}}$  to be significantly different from the reactivity weighted sediment  $\varepsilon_{\text{Nd}}$  that is expressed in the pore water (and therefore the altered bottom water in scenario 2 and directly into the authigenic phase in scenario 3). The highly-reactive sediment component preferentially contributes  $\varepsilon_{\text{Nd}}$  to the fluid phase and can make up a significant portion of the neodymium in the fluid even as a minor sediment component since the pore water is typically  $< 0.001\%$  of the neodymium in the surrounding solid reservoir (Abbott et al., 2016). At the same time, because of its small presence the minor component does not have a similar impact on the total sediment  $\varepsilon_{\text{Nd}}$  and may be a small enough fraction to remain undetected in sediment mineralogy using XRD (Abbott et al., 2019). Therefore, if this reactive component has an  $\varepsilon_{\text{Nd}}$  that is sufficiently distinct from that of the bulk sediment we would expect an offset between authigenic  $\varepsilon_{\text{Nd}}$  (determined by the reactive components) and detrital (bulk)  $\varepsilon_{\text{Nd}}$  in scenarios 2 or 3, especially if the reactive component is only present in trace amounts (e.g. Wilson et al., 2012; Pearce et al., 2013; Wilson et al., 2013; Jeandel and Oelkers, 2015; Abbott et al., 2016). This means that the authigenic archive, even sourcing its signature entirely from the pore water whether directly (scenario 3) or via altered bottom water (scenario 2), can be decoupled from the detrital (bulk)  $\varepsilon_{\text{Nd}}$  signature (i.e. bottom water  $\varepsilon_{\text{Nd}} =$  pore water  $\varepsilon_{\text{Nd}} =$  reactivity weighted detrital  $\neq$  bulk sediment).

The scenarios we consider focus on processes at or near the sediment water interface because an increasing body of literature suggests that the sediments are a significant driver of ocean Nd cycling (Arsouze et al., 2009; Rempfer et al., 2011; Haley et al., 2017; Abbott et al., 2019) whereas water column processes such as reversible scavenging have a relatively minor role in balancing the neodymium budget because they merely redistribute Nd within the water column but do not introduce the new net Nd source required to balance the modern budget (Arsouze et al., 2009). Furthermore, neither the magnitude nor geographic pattern

of non-conservative  $\varepsilon_{\text{Nd}}$  behavior correlate well to surface water  $\varepsilon_{\text{Nd}}$  as would be predicted by the reversible scavenging model; instead, these show a strong correlation to sea-floor detrital  $\varepsilon_{\text{Nd}}$  (Du et al., 2020), more consistent with a bottom-up control. The limited role of reversible scavenging on the overall marine Nd budget is further supported by modeling experiments which have shown little change to  $\varepsilon_{\text{Nd}}$  with variations to the particle fields (Gu et al., 2019).

## 4. DISCUSSION

### 4.1. Global Trends

The strong correlation between authigenic and detrital phases globally (Fig. 2) is inconsistent with authigenic  $\varepsilon_{\text{Nd}}$  as strictly a bottom water tracer (‘traditional’ scenario, Section 3.4, Fig. 6a), and instead suggests that the authigenic signal is, at least in part, controlled by the provenance of the detrital sedimentary material and terrestrial weathering (Fig. 6b, 6c; Groussset et al., 1988; Abbott et al., 2016; Du et al., 2016; Haley et al., 2017; Bayon et al., 2020; Du et al., 2020; Robinson et al., 2021). The consistency of this correlation across ocean basins, time periods, and multiple authigenic archives including fish teeth/debris, foraminifera, and the acid leachable component of the sediment, despite a range of methods to access the authigenic fraction (Supplemental Table 3), demonstrates that such a correlation is not simply an artifact associated with sediment leaching protocols that tap into an ‘unintentional phase’ (e.g. Wilson et al., 2013; Du et al., 2016; McKinley et al., 2019). Similarly the coverage of this compilation demonstrates the correlation is not a spatially or temporally limited phenomenon restricted to areas with particularly reactive detritus or times of high ice rafted debris deposition (e.g. Roberts and Piotrowski, 2015; Howe et al., 2016; Blaser et al., 2019). Additionally, this global marine correlation closely resembles the correlation between the leachable fraction and corresponding detritus observed in rivers draining crystalline, volcanic, and mixed lithological watersheds (Bayon et al., 2020).

We argue that this multi-record compilation demonstrates widespread control of authigenic neodymium signatures by a detrital (lithogenic) influence, either indirectly through benthic flux alteration of bottom water (scenario 2, Fig. 6b) or directly through isotopic exchange with the pore water during early diagenesis (scenario 3, Fig. 6c; e.g. Pearce et al., 2013; Abbott et al., 2016; Huck et al., 2016; Skinner et al., 2019; Du et al., 2020). Either scenario 2 or 3 could result in the observed high correlation coefficients between the authigenic and detrital records. Looked at individually, all three authigenic archives (fish teeth/debris, sediment leaches, and foraminifera records) are strongly correlated with their paired detrital record (Table 1) and all generally fall close to a 1:1 slope (Fig. 2).

We expect that the degree to which a paired record is correlated is a function of the extent of detrital influence, with scenario 3 resulting in the highest correlation coefficient and scenario 1 the lowest. We further suggest that the degree to which the authigenic  $\varepsilon_{\text{Nd}}$  and detrital  $\varepsilon_{\text{Nd}}$  are decoupled (e.g.  $\Delta\varepsilon_{\text{Nd}}$ , Bayon et al., 2020) may reflect

the relative importance of scenario 1 over scenario 2 or 3, or in the absence of scenario 1 is a function of the contribution of a small but highly reactive and isotopically distinct sediment component (scenario 2 or 3) and upstream influences (via scenario 2) as we will demonstrate for ODP site 1063 and IODP site 1308 in [Section 4.2](#). For instance, radiogenic offsets of the authigenic archive resulting from differential dissolution of reactive Nd-containing sediment phases (e.g. Tachikawa et al., 2004; Jeandel et al., 2007; Wilson et al., 2012; Pearce et al., 2013; Wilson et al., 2013; Osborne et al., 2014; Rousseau et al., 2015; Jeandel and Oelkers, 2015; Abbott et al., 2016; Du et al., 2016; McKinley et al., 2019) are evident in records from semi-enclosed basins (e.g. Mediterranean and Caribbean, [Fig. 2G](#)). These offsets are consistent with observations of a reactive radiogenic phase in less compositionally mature (i.e. less chemically weathered) sediments and along continental margins (e.g. Abbott et al., 2016; Zhao et al., 2019) and the longer exposure time for bottom waters in restricted basins would amplify this effect in the benthic flux scenario (e.g. Osborne et al., 2014). Furthermore, there is well-documented evidence of volcanic derived material in both the Mediterranean and Caribbean (Krom et al., 2002; Weldeab et al., 2002; Jeandel et al., 2007; Osborne et al., 2014) and in the North Atlantic region influenced by Icelandic volcanics as discussed below.

#### 4.2. Case Study: LGM in the North Atlantic

We evaluate two sites in the North Atlantic (ODP 1063 and IODP 1308, [Fig. 1](#)) across the Last Glacial and Last Deglaciation using our new interpretative framework and high-resolution SEM-EDS based mineral mapping to examine mechanistic drivers of the correlation between the authigenic and bulk sediment  $\epsilon_{\text{Nd}}$  records ([Fig. 3](#)). This part of Earth's history is characterized by rapid climate oscillations accompanied by massive reorganisations of global ocean circulation (Böhm et al., 2015; Jonkers et al., 2015).

##### 4.2.1. Site 1308

The prevalence of ice rafted debris (IRD) at IODP site 1308 during the Heinrich Events has led previous studies to investigate the detrital influence in the neodymium records from this site. Specifically, the negative excursions in authigenic  $\epsilon_{\text{Nd}}$  records have been attributed to reactive detritus (Blaser et al., 2019; Vogt-Vincent et al., 2020), despite similar negative excursions elsewhere in the Atlantic being interpreted as shifts in the Atlantic Meridional Overturning Circulation (Roberts et al., 2010; Wilson et al., 2014; Böhm et al., 2015) or a changing  $\epsilon_{\text{Nd}}$  of the Labrador Sea end-member (Vance and Burton, 1999). Going back to the onset of Northern Hemisphere glaciation, Von Blanckenburg and Nägler (2001) provide an explanation for such an isotopic shift suggesting that the incongruent release of a labile fraction during Northern Hemisphere glaciations results in a highly unradiogenic neodymium signature due to the continental detritus eroding into the Labrador Sea and that the transition from chemical weathering to mechanical erosion alone is enough to result in signifi-

cant variations in the ocean's radiogenic tracers. We argue that this detrital impact is not restricted to the IRD layers of the Heinrich Events. Instead, we suggest that the detrital impact from IRD is simply the most noticeable detrital influence. The large difference between the highly unradiogenic  $\epsilon_{\text{Nd}}$  of the IRD and the background sedimentation, which more closely resembles expected deep water values, makes the influence of such detritus more apparent whether it is through a reaction with the bottom water or after deposition (e.g. Abbott et al., 2015b; Howe et al., 2016; Blaser et al., 2019; Vogt-Vincent et al. 2020).

Overall, the authigenic  $\epsilon_{\text{Nd}}$  records available at IODP 1308 generally follow the same trends as our bulk sediment  $\epsilon_{\text{Nd}}$  data suggesting the authigenic record is influenced by the sediments throughout the last 55 kyr ([Fig. 3](#), [Fig. 5](#)). An excursion to less radiogenic  $\epsilon_{\text{Nd}}$  values in both the authigenic and bulk sediment records from IODP 1308 is apparent at Heinrich Events 1 and 2 ([Fig. 3](#)). This excursion to less radiogenic  $\epsilon_{\text{Nd}}$  values is also apparent in bulk sediments records from Heinrich Events 4 and 5 but no corresponding authigenic  $\epsilon_{\text{Nd}}$  data are available ([Fig. 5](#)). One sedimentary component that may be responsible for the unradiogenic response during Heinrich Events is IRD from the North American Laurentian ice sheet (e.g. Broecker et al., 1992; Hemming, 2004; Roberts and Piotrowski, 2015; Blaser et al., 2019) and our SEM images confirm the presence of IRD during these intervals. This IRD consists of lithic clasts of both igneous and meta-sedimentary origin, as well as detrital carbonates (calcite, dolomite), feldspar, and quartz clasts ([Fig. 3](#); [Fig. 5](#)). While smaller meta-sedimentary lithics can be identified in Heinrich Events 1 and 2, the most prevalent meta-sedimentary clasts are found during Heinrich Event 5 ([Fig. 5](#); note that only a subset of samples were imaged, [Supplemental Table 2](#)). These meta-sedimentary clasts contain abundant chlorite, an iron rich clay mineral thought to play an important role in moderating pore water rare earth elements (Abbott et al., 2019). In addition to chlorite, they also contain feldspar, quartz and mica ([Fig. 5](#)). Likely originating from a North American source (e.g. Broecker et al., 1992; Hemming, 2004), the neodymium associated with the chlorite can reasonably be assumed to carry a highly unradiogenic signature. These clasts likely preferentially bias sediment leachates towards more unradiogenic values, even in small quantities as seen at Heinrich Event 1 and Heinrich Event 2, as we would expect them to be quite reactive (von Blanckenburg and Nägler, 2001; Homoky et al., 2016; Abbott et al., 2019). In greater quantities, such as observed during Heinrich Event 5, this unradiogenic component would also explain the stronger excursion in the bulk  $\epsilon_{\text{Nd}}$  signature ([Fig. 5](#)).

The correlation between the authigenic  $\epsilon_{\text{Nd}}$  and bulk sediment  $\epsilon_{\text{Nd}}$  downcore suggests that the authigenic  $\epsilon_{\text{Nd}}$  record is not recording bottom water over the last 55 kyr, and instead is being largely determined by the sediments through scenario 2 or 3. The clear sediment compositional changes may indicate a dominant role of the diagenetic scenario (scenario 3) at site 1308 however, the presence of reactive sediment phases would likely also drive an active benthic flux (scenario 2), consistent with estimates of a ben-

thic flux nearly two times the flux estimated in the modern North Pacific during Heinrich Event 1 ( $50 \text{ pmol cm}^{-2} \text{ a}^{-1}$ ; Blaser et al., 2019). A slowdown of the Atlantic Meridional Overturning Circulation at this time would further exaggerate the influence of a benthic flux by increasing the exposure time in scenario 2 (Abbott et al., 2015b; Du et al., 2016; Blaser et al., 2019; McKinley et al., 2019).

Throughout the record, Heinrich Events correspond to both the most unradiogenic bulk and authigenic  $\varepsilon_{\text{Nd}}$  values, whereas adjacent, non-Heinrich, glacial sediments correspond to relatively more radiogenic bulk and authigenic values (Fig. 3; Fig. 5). Despite this overall consistency in trends between authigenic  $\varepsilon_{\text{Nd}}$  and bulk sediment  $\varepsilon_{\text{Nd}}$  downcore, there are some noticeable differences between the two records. We argue these differences are not indicative of an intermittent prevalence of scenario 1, but rather that these differences are due to the presence of reactive phases in the sediments preferentially contributing to the reactive  $\varepsilon_{\text{Nd}}$  pool (Fig. 5, Supplemental Table 3). As discussed in Section 3.4, small abundances of an isotopically unique and reactive material (detrital clays, oxides, or volcanics) would be expected to strongly influence the authigenic  $\varepsilon_{\text{Nd}}$  signatures in scenario 2 or 3 while not noticeably impacting the residual or detrital  $\varepsilon_{\text{Nd}}$  signatures (e.g. Roberts et al., 2010; Wilson et al., 2012; Abbott et al., 2016; Du et al., 2016). For example, if we look at the record prior to 10 kyr, the authigenic  $\varepsilon_{\text{Nd}}$  during glacial but non-Heinrich times is consistently more radiogenic than the detrital  $\varepsilon_{\text{Nd}}$  (Blaser et al. 2019; Fig. 3). This offset between authigenic and detrital  $\varepsilon_{\text{Nd}}$  is likely due to the influence of Icelandic derived material (oxides or clays, potentially volcanic glass or ash; e.g. Roberts and Piotrowski, 2015; Blaser et al., 2019). Such a preferential release of rare earth elements from more reactive sediment components is well documented in the laboratory and in the field (Elmore et al., 2011; Wilson et al., 2012; Pearce et al., 2013; Jeandel and Oelkers, 2015; Rousseau et al., 2015; Abbott et al., 2016). Similarly, the muted bulk isotopic response to Heinrich Event 1 ( $\varepsilon_{\text{Nd}} -14.0$ ) and Heinrich Event 2 ( $\varepsilon_{\text{Nd}} -14.6$ ) compared to the bulk isotopic response to Heinrich 5 ( $\varepsilon_{\text{Nd}} -23.2$ ) is consistent with the most IRD apparent in Heinrich 5 (relatively higher proportion of the bulk). In addition to the chlorite rich IRD, the detrital carbonates are likely also a source of Laurentian sourced unradiogenic neodymium during Heinrich Events (e.g. Roberts and Piotrowski, 2015; Blaser et al., 2019) that would likely be preferentially released during chemical leaching and therefore included in the operationally defined ‘authigenic phase’. The abundance of these detrital carbonates likely overwhelms the more radiogenic  $\varepsilon_{\text{Nd}}$  Iceland-derived signature of the Heinrich events during leaching, particularly with a relatively weak leach solution.

#### 4.2.2. Site 1063

While Site 1063 appears sheltered from the brunt of the Heinrich Event ice discharges, with no noticeable  $\varepsilon_{\text{Nd}}$  excursions, IRD, or mineralogical shifts during the last glaciation, the onset of the Holocene and retreat of the Laurentide Ice Sheet is clearly visible in this record. The authigenic  $\varepsilon_{\text{Nd}}$  record from site 1063 has previously been

interpreted to record a rapid shift in both bottom water source and overturning rates at this deglacial transition (Roberts et al., 2010). The fact that the  $\varepsilon_{\text{Nd}}$  of uncleared foraminifera did not reach the southern source water end-member value during the last glacial has been interpreted as evidence that some proportion of northern source water was maintained, and that the Atlantic Meridional Overturning Circulation did not completely shut down despite higher  $^{231}\text{Pa}/^{230}\text{Th}$  values (Roberts et al., 2010; Böhm et al., 2015). Furthermore, the authigenic (foraminifera)  $-16 \varepsilon_{\text{Nd}}$  during the deglacial transition was interpreted as evidence for an increased proportion of Labrador Sea water in the northern sourced water (Roberts et al., 2010). Interestingly, sediment leaches were dismissed as contaminated based on these leaches returning more radiogenic values when compared to foraminifera, with the assumption being made that the leaches were more heavily impacted by contamination from the detrital phases than the other authigenic records (Roberts et al., 2010). But when we measure the bulk sediment at this site, it is instead the foraminifera that most closely track the sediment values and the leach that is not as tightly coupled, potentially due to the unintentional dissolution of radiogenic volcanic material (Fig. 4). We now consider how our interpretative framework can resolve this discrepancy.

During the last glaciation, the sediments at Bermuda Rise are characterized by fewer marine carbonates than during the deglacial transition or the Holocene (carbonate lean mud, Supplemental Table 3; Fig. 3). The bulk sediment  $\varepsilon_{\text{Nd}}$  during this interval is relatively constant ( $-12$ ), consistent with previously published authigenic  $\varepsilon_{\text{Nd}}$  from the site (Fig. 3, Fig. 4). The sediment is typically fine grained with dominantly clay-sized particles. However, both the bulk sediment and the foraminifera records show a transition to the least radiogenic values by the early Holocene (Fig. 4). This transition in  $\varepsilon_{\text{Nd}}$  begins during the Bølling Allerød and corresponds to a compositional change from carbonate lean muds present until 14.9 kyr to calcareous muds by 12.3 kyr (Supplemental Table 3). We can understand these shifts by examining the behavior of the nearby Laurentide Ice Sheet as well as the changes in AMOC occurring as we move out of the Last Glacial Maximum through Heinrich Stadial 1, the Bølling Allerød Event, the Younger Dryas and into the Holocene (Fig. 4).

During this transition from more radiogenic carbonate lean muds to less radiogenic calcareous muds, the Laurentide Ice Sheet was actively retreating with the St Lawrence Seaway opening by about 11.5 kyrs (Fig. 4; Margold et al., 2018). Accompanying the ice sheet’s retreat and this ‘new’ drainage to the east we expect an influx of fresh unradiogenic material off the Canadian Shield, consistent with records of relatively unweathered sediments entering the abyssal ocean in the proximity of the Labrador Sea during the Bølling Allerød and early Holocene (Fairbanks, 1989; and experimentally demonstrated by von Blanckenburg and Nägler, 2001 for 2.7 Ma). This material from the Canadian Shield, including detrital carbonates, drove the bulk  $\varepsilon_{\text{Nd}}$  to more negative values by 10.7 kyr. The dominance of glacial processes in the region prior to this means that this material experienced only limited chemical weathering

and would therefore have been prone to dissolution (von Blanckenburg and Nägler, 2001; Vance et al., 2009; Zhao et al., 2019), resulting in pore water that resembles the bulk  $\varepsilon_{\text{Nd}}$  values, as demonstrated by the striking resemblance of our bulk  $\varepsilon_{\text{Nd}}$  data with the foraminifera  $\varepsilon_{\text{Nd}}$  data from Roberts et al. (2010) (Fig. 3, Fig. 4). The clear covariation between the bulk and foraminiferal data implies a dominant role for the diagenetic scenario (scenario 3), or a large benthic flux (scenario 2).

Authigenic records from foraminifera and our sediment leachates are similar at site 1063 prior to  $\sim 12$  kyr, however our sediment leachates shift away from the foraminiferal record to more radiogenic values following the Younger Dryas (closer resemblance to the leaches of Roberts et al., 2010; Fig. 4). Coming out of the Younger Dryas into the early Holocene the foraminifera  $\varepsilon_{\text{Nd}}$  tracks the bulk sediment to more unradiogenic values ( $\varepsilon_{\text{Nd}} - 16$ ) while our sediment leachates remain closer to those  $\varepsilon_{\text{Nd}}$  values observed during the last glacial ( $\varepsilon_{\text{Nd}} - 11$ ) after a brief negative excursion ( $\varepsilon_{\text{Nd}} - 13.3$ ) during the Bølling Allerød event at 13.9 kyr (corresponding to the transitional composition sample, Supplemental Table 3). The decoupling of bulk versus authigenic could be interpreted as evidence that the leachate values are recording a signature that is more reflective of bottom-water (i.e. scenario 1 of the interpretative framework; Fig. 6a), perhaps due to the early diagenetic formation of hydrogenetic (oxy)hydroxides (Bayon et al., 2004), whereas the foraminifera are incorporating a reactivity-weighted detrital signature from the pore water during early diagenesis (Skinner et al., 2019). Alternatively, this decoupling may reflect the outsized influence of sediment components that are consistently present at Site 1063 and are mobilized during leaching but do not interact with the pore water under ambient conditions, in which case the foraminifera appear to be a reliable recorder of pore water  $\varepsilon_{\text{Nd}}$ . This hypothesis is consistent with the offset between the sediment leach recovered through a more aggressive leaching protocol (Roberts et al., 2010) being further offset from bulk sediment and pore water values than our weaker leaching protocol after Blaser et al. (2019) which would not attack as many of these phases. The potential issues with sediment leaching ranging from the recovery of such unintentional phases to complications associated with the wide variety of methods applied have been well documented (e.g. Supplemental Table 1; Wilson et al., 2012; Wilson et al., 2013; Abbott et al., 2016; Abbott et al., 2019; McKinley et al., 2019). The complications arising from the operationally defined recovery of phases through sediment leaches is likely why the authigenic values from sediment leaches have the lowest correlation coefficient of the authigenic records examined in our global compilation.

#### 4.3. Reconciling Non-Conservative $\varepsilon_{\text{Nd}}$ with Circulation Reconstructions

If authigenic  $\varepsilon_{\text{Nd}}$  records are largely determined by a sedimentary signature as the data from these two sites and the global compilation would suggest, then why do authigenic  $\varepsilon_{\text{Nd}}$  archives align with independent estimates of circulation changes during past climate perturbations?

While not the traditional bottom water tracer interpretation, both the benthic flux and diagenetic scenarios are sensitive to changes in climate and circulation. This idea is most clearly illustrated at site 1308, where climatic (Heinrich) events resulted in a changed sediment provenance, and hence a sediment compositional and isotopic shift. Whether the authigenic  $\varepsilon_{\text{Nd}}$  is determined in the water column (benthic flux), in the sediment column (diagenetic), or a combination of both, the sediment composition is likely capturing climate driven changes to weathering and transport rates, reactive land area (partially controlled by sea level), ocean circulation, and atmospheric circulation (dust). While speculative, a discussion of potential reasons for authigenic  $\varepsilon_{\text{Nd}}$  correlation to climatic shifts helps to highlight gaps in our understanding of the applicability of this proxy that merit future evaluation.

Processes that could impact sedimentary  $\varepsilon_{\text{Nd}}$  with climatic shifts include both oceanic and terrestrial. For instance, ocean currents are the primary control on the distribution of detrital sediments, particularly the finer grain sizes (Grouset et al., 1988; Revel et al., 1996; Innocent et al., 2000) as illustrated by the southward bound sediment plume of unradiogenic particles from the Labrador Sea visible in both detrital and authigenic phases from core top sediments (Fig. 2). This sediment plume agrees well with the modern water mass movement from the Labrador Sea identified by dissolved and particulate  $\varepsilon_{\text{Nd}}$  (Lambelet et al., 2016; Stichel et al., 2020). Furthermore, climate will influence dust abundance and source region (e.g. formerly submerged continental shelf becomes prone to deflation by wind during sea level lows; Hesse and McTainsh, 2003; Li et al., 2010) and changes to continental weathering will impact sediment composition (Erhmann and Mackensen, 1992; Revel et al., 1996; von Blanckenburg and Nägler, 2001; Anderson et al., 2019; Robinson et al., 2021). In terms of the clay minerals, likely to be an important source of neodymium to the pore water (Abbott et al., 2019; Paul et al., 2019), changes in sediment origin or composition are expected to coincide with climatic shifts. For example, the transition between chemical and mechanical weathering during glacial-interglacial cycles results in significant variation in continental weathering which can result in a shifting isotopic signature from the incongruent release of more labile fractions from the eroding continental detritus (von Blanckenburg and Nägler, 2001). For instance, a decrease in smectite during glacial periods is associated with decreased chemical weathering and increased ice coverage (Erhmann and Mackensen, 1992; Revel et al., 1996). Furthermore, the grain size differences between clay minerals may result in differential transport distances once they reach the ocean, with finer grained smectites carried further from their source than more-coarse-grained kaolinite (Chamley, 1989). Additionally, changes to water movement can be expected to impact the distribution of sediment within a basin and therefore impact  $\varepsilon_{\text{Nd}}$  as a function of sediments reaching a location with different provenance, or sediment composition/reactivity. This idea is supported by the widespread use of  $\varepsilon_{\text{Nd}}$  as a sediment provenance tracer (Grouset et al., 1988; Revel et al., 1996; Franzese et al., 2006; Jeandel et al., 2007),

the observed correlation between authigenic and detrital  $\varepsilon_{\text{Nd}}$  (Fig. 1, Fig. 2), observations that high-resolution elemental records demonstrate concurrent changes in bulk Ti/Ca and  $\varepsilon_{\text{Nd}}$  (1063, Gutjahr and Lippold, 2011), and grain size (circulation) dependent changes in  $\varepsilon_{\text{Nd}}$  distributions (Revel et al., 1996; Innocent et al., 2000).

The combination of mechanistic drivers which impact on the authigenic  $\varepsilon_{\text{Nd}}$  record discussed above mean that even though authigenic  $\varepsilon_{\text{Nd}}$  aligns with independent estimates of shifts in ocean circulation, care must be taken not to interpret authigenic  $\varepsilon_{\text{Nd}}$  as strictly a climate or circulation proxy unless an attempt is made to isolate the intertwined roles of changing sediment sources (composition, reactivity, resulting benthic flux) from shifts in ocean circulation (provenance, exposure time) and regional environmental conditions (productivity, pH). Some of these factors remain poorly constrained in the modern ocean and unconstrained for the oceans of the past. Furthering our understanding of the factors controlling the benthic flux in the modern ocean with the goal to be able to estimate past flux distribution and magnitude, coupling  $\varepsilon_{\text{Nd}}$  with circulation speed records to constrain relative shifts in exposure time, and determining when authigenic phases inherit their  $\varepsilon_{\text{Nd}}$  signature will address some of the current gaps hampering interpretations of authigenic  $\varepsilon_{\text{Nd}}$  and inform future applications of these records.

## 5. CONCLUSIONS

This study demonstrates that the lithogenic influence on marine authigenic  $\varepsilon_{\text{Nd}}$  archives, whether directly in the sediment column or indirectly via the benthic flux, is widespread. We observe similar influences of detrital  $\varepsilon_{\text{Nd}}$  on all types of authigenic records, with similarly high correlation coefficients between the detrital  $\varepsilon_{\text{Nd}}$  and the  $\varepsilon_{\text{Nd}}$  of foraminifera, fish teeth/debris, and sediment leaches. Using isotope records coupled with high-resolution mineral maps, we illustrate sediment composition shifts concurrent with isotopic excursions during Heinrich Events 1, 2, 4, and 5 in the North Atlantic at site 1308. While mineralogical shifts are observed at site 1063 over the deglacial concurrent with the  $\varepsilon_{\text{Nd}}$  shift observed in both the detrital record and the foraminifera record, the inconsistency between authigenic records recorded from leaching and those from foraminifera at this site demonstrate the complexity of interpreting authigenic values obtained through sediment leaching due to the uncertainty of the phases targeted during leaching procedures (Abbott et al., 2016; Du et al., 2016; McKinley et al., 2019). Combined with our global compilation of authigenic and detrital records, these observations demonstrate marine authigenic  $\varepsilon_{\text{Nd}}$  records are not independent of the  $\varepsilon_{\text{Nd}}$  (detrital) of the host sediment. We therefore argue that sediment characteristics and detrital isotope records must be considered when reconstructing past ocean and climate conditions from neodymium isotope records. We propose an interpretative framework allowing for mixed contributions of three end-member scenarios that explicitly articulates the mechanisms determining the extent to which authigenic  $\varepsilon_{\text{Nd}}$  is dependent on sediment characteristics versus bottom water composition. Similar ambigu-

ties around the influence of seafloor cycling on other trace elements and their isotopes (Homoky et al., 2016), increasing evidence for the impact of sediment dissolution on ocean chemistry and global element cycles (Jeandel and Oelkers, 2015), and preliminary work suggesting detrital influence on authigenic phases for isotope systems such as chromium (Frank et al., 2020; Janssen et al., 2021), nickel (Gueguen and Rouxel, 2021) and iron (Abadie et al., 2017), suggest this framework will likely prove widely applicable as more data become available.

## Declaration of Competing Interest

The authors declare that they have no known competing financial interests or personal relationships that could have appeared to influence the work reported in this paper.

## ACKNOWLEDGMENTS

The authors would like to thank the International Ocean Discovery Program (IODP) which provided the samples, and the Australia-New Zealand IODP Consortium (ANZIC), which provided the Legacy funding grant to A.N.A. and S.C.L. for this study. ANZIC is supported by the Australian Government through the Australian Research Council's LIEF funding scheme [LE160100067]. The authors would also like to thank Peter Wieland, Russell Field, Cassandra Wheeler, Samantha Coker, Hannah Wilson, Sean Murray, and Damian Gore for laboratory assistance and Lucy McGee for useful feedback on this manuscript. We also thank the three anonymous reviewers, associate editor F. Marcattonio, and executive editor J.G. Catalano for their time and effort in improving this manuscript.

## APPENDIX A. SUPPLEMENTARY MATERIAL

**Supplementary Material:** This file contains one figure and the complete list of references for data used in the authigenic and detrital correlation presented in the main text (Figure 2). Supplemental figure 1 shows the influence of Casse et al. data on the overall authigenic and detrital correlation.

**Research Data:** This file contains four data tables. Supplementary Table 1 provides a list of the locations and type of records included in the authigenic and detrital correlation, as well as a brief description of the method used by each publication. Supplementary Table 2 lists the full sample names for the sediment samples analysed on SEM-EDS. Supplementary Table 3 presents the core depth, age, measured  $\varepsilon_{\text{Nd}}$  and XRD based lithofacies for each sample analysed from both sites 1063 and 1308. Supplementary Table 4 contains the raw XRD data for each sample.

Supplementary data to this article can be found online at <https://doi.org/10.1016/j.gca.2021.11.021>.

## REFERENCES

- Abadie C., Lacan F., Radic A., Pradoux C. and Poitrasson F. (2017) Iron isotopes reveal distinct dissolved iron sources and pathways in the intermediate versus deep Southern Ocean. *Proc. Natl. Acad. Sci.* **114**, 858–863.

- Abbott A. N., Haley B. A., McManus J. and Reimers C. (2015a) The sedimentary flux of dissolved rare earth elements to the ocean. *Geochim. Cosmochim. Acta* **154**, 186–200.
- Abbott A. N., Haley B. A. and McManus J. (2015b) Bottoms up: sedimentary control of the deep North Pacific Ocean's  $\varepsilon_{\text{Nd}}$  signature. *Geology* **43**, 1035–1038.
- Abbott A. N., Haley B. A. and McManus J. (2016) The impact of sedimentary coatings on the diagenetic Nd flux. *Earth Planet. Sci. Lett.* **449**, 217–227.
- Abbott A. N. (2019) A benthic flux from calcareous sediments results in non-conservative neodymium behavior during lateral transport: A study from the Tasman Sea. *Geology* **47**, 363–366.
- Abbott A. N., Löhr S. and Trethewy M. (2019) Are clay minerals the primary control on the oceanic rare Earth element budget? *Front. Mar. Sci.* **6**, 504.
- Anderson C. H., Murray R. W., Dunlea A. G., Giosan L., Kinsley C. W., McGee D. and Tada R. (2019) Aeolian delivery to Ulleung Basin, Korea (Japan Sea), during development of the East Asian Monsoon through the last 12 Ma. *Geol. Mag.* **157**, 806–817.
- Arsouze T., Dutay J.-C., Lacan F. and Jeandel C. (2009) Reconstructing the Nd oceanic cycle using a coupled dynamical – biogeochemical model. *Biogeosciences* **6**, 2829–2846.
- Basak C., Fröllje H., Lamy F., Gersonde R., Benz V., Anderson R. F., Molina-Kescher M. and Pahnke K. (2018) Breakup of last glacial deep stratification in the South Pacific. *Science* **359** (6378), 900–904.
- Bayon G., German C. R., Burton K. W., Nesbitt R. W. and Rogers N. (2004) Sedimentary Fe-Mn oxyhydroxides as paleoceanographic archives and the role of Aeolian flux in regulation oceanic dissolved REE. *Earth Planet. Sci. Lett.* **224**, 477–492.
- Bayon G., Lambert T., Vigier N., De Deckker P., Freslon N., Jang K., Larkin C. S., Piotrowski A. M., Tachikawa K., Thollon M. and Tipper E. T. (2020) Rare earth element and neodymium isotope tracing of sedimentary rock weathering. *Chem. Geol.* **553** 119794.
- Blaser P., Lippold J., Gutjahr M., Frank N., Link J. M. and Frank M. (2016) Extracting foraminiferal seawater Nd isotope signatures from bulk deep sea sediment by chemical leaching. *Chem. Geol.* **439**, 189–204.
- Blaser P., Pöppelmeir F., Schulz H., Gutjahr M., Frank M., Lippold J., Heinrich H., Link J. M., Hoffman J., Szidat S. and Frank N. (2019) The resilience and sensitivity of Northeast Atlantic deep water  $\varepsilon_{\text{Nd}}$  to overprinting by detrital fluxes over the past 30,000 years. *Geochim. Cosmochim. Acta* **245**, 79–97.
- Böhm E., Lippold J., Gutjahr M., Frank M., Blaser P., Antz B., Fohlmeister J., Frank N., Andersen M. B. and Deininger M. (2015) Strong and deep Atlantic meridional overturning circulation during the last glacial cycle. *Nature* **517**, 73–76.
- Broecker W., Bond G., Klas M., Clark E. and McManus J. (1992) Origin of the northern Atlantic's Heinrich events. *Clim. Dyn.* **6**, 265–273.
- Casse M., Montero-Serrano J.-C., St-Onge G. and Poirier A. (2019) REE Distribution and Nd isotope composition of estuarine waters and bulk sediment leachates tracing lithogenic inputs in eastern Canada. *Mar. Chem.* **211**, 117–130.
- Chamley H. (1989) Chapter 6 Clay Sorting and Settling in the Ocean. In *Clay Sedimentology*. Springer-Verlag, Berlin Heidelberg New York, pp. 117–131.
- Crocker A. J., Chalk T. B., Bailey I., Spencer M. R., Gutjahr M., Foster G. L. and Wilson P. A. (2016) Geochemical response of the mid-depth Northeast Atlantic Ocean to freshwater input during Heinrich events 1 to 4. *Quat. Sci. Rev.* **151**, 236–254.
- Du J., Haley B. A. and Mix A. C. (2016) Neodymium isotopes in authigenic phases, bottom waters and detrital sediments in the Gulf of Alaska and their implications for paleo-circulation reconstruction. *Geochim. Cosmochim. Acta* **193**, 14–35.
- Du J., Haley B. A. and Mix A. C. (2020) Evolution of the Global Overturning Circulation since the Last Glacial Maximum based on marine authigenic neodymium isotopes. *Quat. Sci. Rev.* **241** 106396.
- Elmore A. C., Piotrowski A. M., Wright J. D. and Scrivner A. E. (2011) Testing the extraction of past seawater Nd isotopic composition from North Atlantic deep sea sediments and foraminifera. *Geochem. Geophys. Geosyst.* **12**, Q09008.
- Ehrmann W. U. and Mackensen A. (1992) Sedimentological evidence for the formation of an East Antarctic ice sheet in Eocene/Oligocene time. *Palaeogeogr. Palaeoclimatol. Palaeoecol.* **93**, 85–112.
- Fairbanks R. G. A. (1989) A 17,000 year glacio-eustatic sea level record: influence of glacial melting rates on the Younger Dryas event and deep-ocean circulation. *Nature* **342**, 637–642.
- Frank M. (2002) Radiogenic isotopes: Tracers of past ocean circulation and erosional input. *Rev. Geophys.* **40**, 1-1-1-38.
- Frank A. B., Klaebe R. M., Löhr S., Xu L. and Frei R. (2020) Chromium isotope composition of organic-rich marine sediments and their mineral phases and implications for using black shales as a paleoredox archive. *Geochim. Cosmochim. Acta* **270**, 338–359.
- Franzese A. M., Hemming S. R., Goldstein S. L. and Anderson R. F. (2006) Reduced Agulhas Leakage during the Last Glacial Maximum inferred from an integrated provenance and flux study. *Earth Planet. Sci. Lett.* **250**, 72–88.
- Grousset F. E., Biscaye P. E., Zindler A., Prospero J. and Chester R. (1988) Neodymium isotopes as tracers in marine sediments and aerosols: North Atlantic. *Earth Planet. Sci. Lett.* **87**, 367–378.
- Gu S., Liu Z., Jahn A., Rempfer J., Zhang J. and Joos F. (2019) Modeling neodymium isotopes in the ocean component of the Community Earth System Model (CESM1). *J. Adv. Model. Earth Syst.* **11**, 624–640.
- Gueguen B. and Rouxel O. (2021) The Nickel isotope composition of the authigenic sink and the diagenetic flux in modern oceans. *Chem. Geol.* **563** 120050.
- Gutjahr M. and Lippold J. (2011) Early arrival of Southern Source Water in the deep North Atlantic prior to Heinrich event 2. *Paleoceanography* **26**, PA2101. doi:10.1029/2011PA002114.
- Gutjahr M., Frank M., Stirling C. H., Keigwin L. D. and Halliday A. N. (2008) Tracing the Nd isotope evolution of North Atlantic Deep and Intermediate Waters in the western North Atlantic since the Last Glacial Maximum from Blake Ridge sediments. *Earth Planet. Sci. Lett.* **266**, 61–77.
- Haberlah D., Löhr S., Kennedy M. J., Debenham N. and Lattanzi D. (2015) Innovative sub-micron SEM-EDS mineral mapping and analysis applied to Australian Shale samples. In *Proceedings of the AAPG International Conference and Exhibition, Melbourne, Australia 13–16 September 2015: SEG Global Meeting Abstracts*. Society of Exploration Geophysicists, Tulsa, OK, p. 419. doi:10.1190/ice2015-2211146.
- Haley B. A., Klinkhammer G. P. and McManus J. (2004) Rare earth elements in pore waters of marine sediments. *Geochim. Cosmochim. Acta* **68**, 1265–1279.
- Haley B. A., Du J., Abbott A. N. and McManus J. (2017) The impact of benthic processes on rare earth element and neodymium isotope distributions in the Oceans. *Front. Mar. Sci.* **4**, 426.
- Hemming S. R. (2004) Heinrich events: massive late Pleistocene detritus layers of the North Atlantic and their global climate imprint. *Rev. Geophys.* **42**, RG 1005.

- Hesse P. P. and McTainsh G. H. (2003) Australian dust deposits: modern processes and the Quaternary record. *Quat. Sci. Rev.* **22**, 2007–2035.
- Hodell D. A., Channel J. E. T., Romero O. E. and Röhl U. (2008) Onset of “Hudson Strait” Heinrich events in the eastern North Atlantic at the end of the middle Pleistocene transition (~640 ka)? *Paleoceanography* **23**, PA4218.
- Hodell D. A., Nicholl J. A., Bontognali T. R. R., Danino S., Dorador J., Dowdeswell J. A., Einsle J., Kuhlmann H., Martrat B., Mlencek-Vautravers M. J., Rodríguez-Tovar F. J. and Röhl U. (2017) Anatomy of Heinrich Layer 1 and its role in the last deglaciation. *Paleoceanography* **32**, 284–303.
- Homoky W. B., Weber T., Berelson W. M., Conway T. M., Henderson G. M., van Hulten M., Jeandel C., Severmann S. and Tagliabue A. (2016) Quantifying trace element and isotope fluxes at the ocean-sediment boundary: a review. *Philos. Trans. R. Soc. London Ser. A* **374**, 20160246.
- Howe J. N. W., Piotrowski A. M. and Rennie V. C. F. (2016) Abyssal origin for the early Holocene pulse of unradiogenic neodymium isotopes in Atlantic seawater. *Geology* **44**, 831–834.
- Huck C. E., van de Flierdt T., Jiménez-Espejo F., Bohaty S. M., Röhl U. and Hammond S. J. (2016) Robustness of fossil fish teeth for seawater neodymium isotope reconstructions under variable redox conditions in an ancient shallow marine setting. *Geochem. Geophys. Geosyst.* **17**, 679–698.
- Innocent C., Fagel N. and Hillaire-Marcel (2000) Sm-Nd isotope systematics in deep-sea sediments: clay-size versus coarser fractions. *Mar. Geol.* **168**, 79–87.
- Jacobsen S. B. and Wasserburg G. J. (1980) Sm-Nd isotopic evolution of chondrites. *Earth Planet. Sci. Lett.* **50**, 139–155.
- Janssen D. J., Rickli J., Abbott A. N., Ellwood M. J., Twining B. S., Ohnemus D. C., Nasemann P., Gilliard D. and Jaccard S. L. (2021) Release from biogenic particles, benthic fluxes, and deep water circulation control Cr and  $\delta^{53}\text{Cr}$  distributions in the ocean interior. *Earth Planet. Sci. Lett.* **574** 117163.
- Jaume-Sequí M., Kim J., Pena L. D., Goldstein S. L., Knudson K. P., Yehudai M., Hartman A. E., Bolge L. and Ferretti P. (2021) Distinguishing glacial AMOC and interglacial non-AMOC Nd isotopic signals in the deep Western Atlantic over the last 1 Myr. *Paleoceanogr. Paleoclimatol.* **36**, PA003877.
- Jeandel C., Arsouze T., Lacan F., Téchiné P. and Dutay J.-C. (2007) Isotopic Nd compositions and concentrations of lithogenic inputs into the ocean: A compilation, with an emphasis on the margins. *Chem. Geol.* **239**, 156–164.
- Jeandel C. and Oelkers E. H. (2015) The influence of terrigenous particulate material dissolution on ocean chemistry and global element cycles. *Chem. Geol.* **395**, 50–66.
- Jeandel C. (2016) Overview of the mechanisms that could explain the ‘Boundary Exchange’ at the land-ocean contact. *Philos. Trans. R. Soc. London, Ser. A* **374**, 20150287.
- Jones K. M., Khatiwala S. P., Goldstein S. L., Hemming S. R. and van de Flierdt T. (2008) Modeling the distribution of Nd isotopes in the oceans using an ocean general circulation model. *Earth Planet. Sci. Lett.* **272**, 610–619.
- Jonkers L., Barker S., Hall I. R. and Prins M. A. (2015) Correcting for the influence of ice-rafterd detritus on grain size-based paleocurrent speed estimates. *Paleoceanography* **30**, 1347–1357.
- Krom M. D., Stanley J. D., Cliff R. A. and Woodward J. C. (2002) Nile River sediment fluctuations over the past 7000 yr and their key role in sapropel development. *Geology* **30**, 71–74.
- Lambelet M., van de Flierdt T., Crocket K., Rehkämper M., Kreissig K., Coles B., Rijkenberg M. J. A., Gerrings L. J. A., de Baar H. J. W. and Steinfeldt R. (2016) Neodymium isotopic composition and concentration in the western North Atlantic Ocean: Results from the GEOTRACES GA02 section. *Geochim. Cosmochim. Acta* **177**, 1–29.
- Li F., Ramaswamy V., Ginoux P., Broccoli A. J., Delworth T. and Zeng F. (2010) Toward understanding the dust deposition in Antarctica during the Last Glacial Maximum: Sensitivity studies on plausible causes. *J. Geophys. Res. D: Atmos.* **115**, D24120.
- Margold M., Stokes C. R. and Clark C. D. (2018) Reconciling records of ice streaming and ice margin retreat to produce a palaeogeographic reconstruction of the deglaciation of the Laurentide Ice Sheet. *Quat. Sci. Rev.* **189**, 1–30.
- McKinley C. C., Thomas D. J., LeVay L. J. and Rolewicz Z. (2019) Nd isotopic structure of the Pacific Ocean 40–10 Ma, and evidence for the reorganization of deep North Pacific Ocean circulation between 36 and 25 Ma. *Earth Planet. Sci. Lett.* **521**, 139–149.
- Ng H. C., Robinson L. F., McManus J. F., Mohamed K. J., Jacobel A. W., Ivanovic R. F., Gregoire L. J. and Chen T. (2018) Coherent deglacial changes in western Atlantic Ocean circulation. *Nature Commun.* **9**, 2947.
- Nijenhuis I. A. and de Lange G. J. (2000) Geochemical constraints on Pliocene sapropel formation in the eastern Mediterranean. *Mar. Geol.* **163**, 41–63.
- Osborne A. H., Haley B. A., Hathorne E. C., Flögel S. and Frank M. (2014) Neodymium isotopes and concentrations in Caribbean seawater: Tracing water mass mixing and continental input in a semi-enclosed ocean basin. *Earth Planet. Sci. Lett.* **406**, 174–186.
- Palmer M. R. and Elderfield H. (1985) Variations in the Nd isotopic composition of foraminifera from Atlantic Ocean sediments. *Earth Planet. Sci. Lett.* **73**, 299–1205.
- Palmer M. R. and Elderfield H. (1986) Rare earth elements and neodymium isotopes in ferromanganese oxide coatings of Cenozoic foraminifera from the Atlantic Ocean. *Geochim. Cosmochim. Acta* **50**, 409–417.
- Paul S. A. L., Haeckel M., Bau M., Bajracharya R. and Koschinsky A. (2019) Small-scale heterogeneity of trace metals including rare earth elements and yttrium in deep-sea sediments and porewaters of the Peru Basin, SE equatorial Pacific. *Biogeosciences* **16**, 4829–4849.
- Pearce C. R., Jones M. T., Oelkers E. H., Pradoux C. and Jeandel C. (2013) The effect of particulate dissolution on the neodymium (Nd) isotope and rare earth element (REE) composition of seawater. *Earth Planet. Sci. Lett.* **369–370**, 138–147.
- Rafiei M., Löhr S. C., Baldermann A., Webster R. and Kong C. (2020) Quantitative petrographic differentiation of detrital vs diagenetic clay minerals in marine sedimentary sequences: Implications for the rise of biotic soils. *Precambrian Res.* **350**, 105948.
- Rempfer J., Stocker T. F., Joos F., Dutay J.-C. and Siddall M. (2011) Modelling Nd-isotopes with a coarse resolution ocean circulation model: Sensitivities to model parameters and source/sink distributions. *Geochim. Cosmochim. Acta* **75**, 5927–5950.
- Revel M., Cremer M., Grousset F. E. and Labeyrie L. (1996) Grain-size and Sr-Nd isotopes as tracer of paleo-bottom current strength, Northeast Atlantic Ocean. *Mar. Geol.* **131**, 233–249.
- Roberts N. L., Piotrowski A. M., McManus J. F. and Keigwin L. D. (2010) Synchronous deglacial overturning and water mass source changes. *Science* **327**, 75–77.
- Roberts N. L. and Piotrowski A. M. (2015) Radiogenic Nd isotope labeling of the northern NE Atlantic during MIS 2. *Earth Planet. Sci. Lett.* **423**, 125–133.
- Robinson S., Ivanovic R., van de Flierdt T., Blanchet C. L., Tachikawa K., Martin E. E., Cook (Falco) C. P., Williams T., Gregoire L., Plancherel Y., Jeandel C. and Arsouze T. (2021)

- Global continental and marine detrital  $\varepsilon_{\text{Nd}}$ : An updated compilation for use in understanding marine Nd cycling. *Chem. Geol.* **567**, 120119.
- Rousseau T. C., Sonke J. E., Chmeleff J., van Beek P., Souhaut M., Boaventura G., Seyler P. and Jeandel C. (2015) Rapid neodymium release to marine waters from lithogenic sediments in the Amazon estuary. *Nat. Commun.* **6**, 7592.
- Rutberg R. L., Hemming S. R. and Goldstein S. L. (2000) Reduced North Atlantic Deep Water flux to the glacial Southern Ocean inferred from neodymium isotope ratios. *Nature* **405**, 935–938.
- Scher H. D. and Martin E. E. (2004) Circulation in the Southern Ocean during the Paleogene inferred from neodymium isotopes. *Earth Planet. Sci. Lett.* **228**, 391–405.
- Seidov D. and Maslin M. (1999) North Atlantic deep water circulation collapse during Heinrich events. *Geology* **27**, 23–26.
- Skinner L. C., Sadekov A., Brandon M., Greaves M., Plancherel Y., de la Fuente M., Gottschalk J., Souane-Ureta S., Sevilgen D. S. and Scrivner A. E. (2019) Rare Earth Elements in early-diagenetic foraminifer ‘coatings’: Pore-water controls and potential palaeoceanographic applications. *Geochim. Cosmochim. Acta* **245**, 118–132.
- Stichel T., Kretschmer S., Geibert W., Lambelet M., Plancherel Y., van der Looff M. R. and van de Flierdt T. (2020) Particle-seawater interaction of neodymium in the North Atlantic. *ACS Earth Space Chem.* **4**, 1700–1717.
- Tachikawa K., Athias V. and Jeandel C. (2003) Neodymium budget in the modern ocean and paleo-oceanographic implications. *J. Geophys. Res.* **108**, 3254.
- Tachikawa K., Roy-Barman M., Thouron M. A., Yeghicheyan D. and Jeandel C. (2004) Neodymium isotopes in the Mediterranean Sea: comparison between seawater and sediment signals. *Geochim. Cosmochim. Acta* **68**, 3095–3106.
- Tachikawa K., Arsouze T., Bayon G., Bory A., Colin C., Dutay J.-C., Frank N., Giraud X., Gourlan A. T., Jeandel C., Lacan F., Meynadier L., Montagna P., Piotrowski A. M., Plancherel Y., Pucéat E., Roy-Barman M. and Waelbroeck C. (2017) The large-scale evolution of neodymium isotopic composition in the global modern and Holocene ocean revealed from seawater and archive data. *Chem. Geol.* **457**, 131–148.
- Van de Flierdt T., Griffiths A. M., Lambelet M., Little S. H., Stichel T. and Wilson D. J. (2016) Neodymium in the oceans: a global database, a regional comparison and implications for palaeoceanographic research. *Philos. Trans. R. Soc. London, Ser. A* **374**, 20150293.
- Vance D. and Burton K. (1999) Neodymium isotopes in planktonic foraminifera: A record of the response of continental weathering and ocean circulation rates to climate change. *Earth Planet. Sci. Lett.* **173**, 365–379.
- Vance D., Teagle D. A. and Foster G. L. (2009) Variable Quaternary chemical weathering fluxes and imbalances in marine geochemical budgets. *Nature* **458**, 493–496.
- Vogt-Vincent N., Lippold J., Kaboth-Bahr S. and Blaser P. (2020) Ice-raftered debris as a source of non-conservative behavior for the  $\varepsilon_{\text{Nd}}$  palaeotracer: Insights from a simple model. *Geo-Mar. Lett.* **40**, 325–340.
- Von Blanckenburg F. and Nägler T. F. (2001) Weathering versus circulation-controlled changes in radiogenic isotope tracer composition of the Labrador Sea and North Atlantic Deep Water. *Paleoceanography* **16**, 424–434.
- Weldeab S., Emeis K.-C. C., Hemleben C., Vennemann T. W. and Schulz H. (2002) Sr and Nd isotope composition of Late Pleistocene sapropels and nonsapropelic sediments from the Eastern Mediterranean Sea. *Geochim. Cosmochim. Acta* **66**, 3585–3598.
- Wilson D. J., Piotrowski A. M., Galy A. and McCave N. (2012) A boundary exchange influence on deglacial neodymium isotope records from the deep western Indian Ocean. *Earth Planet. Sci. Lett.* **341–344**, 35–47.
- Wilson D. J., Piotrowski A. M., Galy A. and Clegg J. A. (2013) Reactivity of neodymium carriers in deep sea sediments: Implications for boundary exchange and paleoceanography. *Geochim. Cosmochim. Acta* **109**, 197–221.
- Wilson D. J., Crocket K. C., van de Flierdt T., Robinson L. F. and Adkins J. F. (2014) Dynamic intermediate ocean circulation in the North Atlantic during Heinrich Stadial 1: A radiocarbon and neodymium isotope perspective. *Paleoceanography* **29**, 1072–1093.
- Zhao N., Oppo D. W., Huang K.-F., Howe J. N. W., Bluszta J. and Keigwin L. D. (2019) Glacial-interglacial Nd isotope variability of North Atlantic Deep Water modulated by North American ice sheet. *Nat. Commun.* **10**, 5773.

*Associate editor:* Franco Marcantonio